# Pictorial Essay
# Benign and Malignant Bone Tumors: Radiological Diagnosis and Imaging Features

**Katharina Grünberg, M.D.; Christoph Rehnitz, M.D.; Marc-André Weber, M.D., M.Sc.**

Section Musculoskeletal Radiology, Diagnostic and Interventional Radiology, University Hospital Heidelberg, Germany

## Topics

The learning objectives of this review article are to identify benign vs. malignant criteria in bone tumor diagnosis and also to differentiate the types of bone tumors and their characterization. Based on the Lodwick classification an overview of the three main types of bone destruction patterns visible on radiographs will be given with many examples. Typical examples of benign and malignant bone tumors will be demonstrated, the various imaging modalities will be compared, and their utility will be discussed. The image gallery comprises pearls and pitfalls. Presentation of standardized magnetic resonance imaging (MRI) protocols will be given. Of course, this pictorial essay does not have the focus of comprehensively presenting all bone tumor entities.

## Introduction

Primary bone tumors are categorized according to their tissue of origin into cartilage, osteogenic, fibrogenic, fibrohistiocytic, haematopoietic, vascular, lipogenic tumors and several other tumors, like Ewing sarcoma and giant cell tumor [1]. Thy are also classified as either benign, malignant or semi-malignant, as well as tumor-like lesions [2]. They are rare, but found on radiographs during an investigation of a painful skeletal region or incidentally, e.g. when performing a joint or whole-body MRI. You will need four diagnostic columns to make a diagnosis of a bone tumor.

---

**1**

## Four diagnostic columns



Tumor's aggressiveness | Tumor matrix | Tumor location | Patient's age
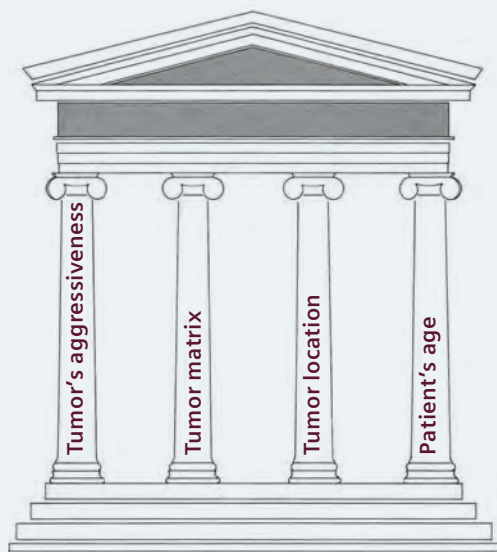
1. **Malignant vs. benign?**
   X-rays:
   Aggressiveness: Analysis of growth rate (Lodwick classification),
   periosteal reaction?
   Further imaging modality → CT, MRI?
   **Make a specific diagnosis:**
2. Analysis of **tumor matrix**: X-rays, CT: Osteolytic, osteoblastic, mixed
3. **Location** within the tumor-bearing bone: Epi-, meta-, diaphysis
4. **Patient's age**, (affected bone)

   in 80% correct specific diagnosis [4]

**1** The four diagnostic columns needed to achieve a correct, specific diagnosis in about 80% of cases [4].

## Four diagnostic columns (Fig. 1)

### Tumor's aggressiveness

The radiograph is the first method to distinguish benign from malignant lesions: at first by analysing the aggressiveness (analysis of growth rate) of a lesion according to the classification of Lodwick [3]. In radiographs there is a correlation between bone tumor's growth rate and dignity. If you identify an aggressive growth pattern and/or malignant periosteal reaction another imaging modality like computed tomography (CT) or magnetic resonance imaging (MRI) is needed. MRI is important for defining the extension of tumor before biopsy.

### Tumor matrix

In a second step, it is essential to analyze the mineralisation of tumor matrix in radiographs or CT. The matrix may be osteolytic, osteoblastic, or mixed, i.e. osteolytic with matrix mineralisation.

### Tumor location and patient age

To make a specific tumor diagnosis, the location within the tumor-bearing bone (epi-, meta- and diaphysis) and the patient's age are also important. With an optimized combination of the different parameters, the expert achieves a correct, specific diagnosis in about 80% of cases [4, 5]. In other words, even a dedicated musculo-skeletal radiologist fails to predict the correct histological diagnosis in one fifth of all cases.

## Lodwick classification (Fig. 2)

Based on the Lodwick classification, an overview of the three main types of bone destruction patterns visible on radiographs are given with a representative example:
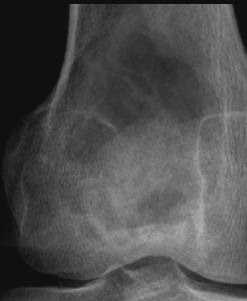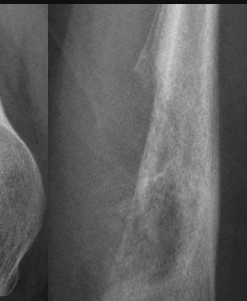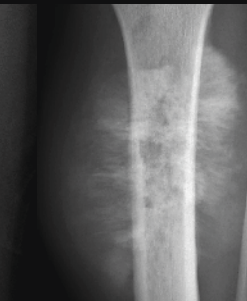
**Type 1:** geographic (with a: well-defined border with sclerotic rim, b: well-defined and sharp border but without sclerotic rim, c: ill-defined and blurred border);

**Type 2:** geographic with moth-eaten or permeated pattern (patchy lysis);

**Type 3:** small, patchy, ill-defined areas of lytic bone destruction with moth-eaten or permeated pattern (patchy lucencies) [3, 6].



### Lodwick classification

| IA | IB | IC | II | III |
|---|---|---|---|---|
| Non-ossifying fibroma | Aneurysmal bone cyst | Giant cell tumor | Osteosarcoma | Ewing's sarcoma |
| Geographic, well-defined & sclerotic rim | Geographic well-defined & sharp border but without sclerotic rim | Geographic but blurred border | Geographic & moth-eaten damage with patchy lysis | Permeated lytic damage with small patchy lucencies |

2　Lodwick classification: An overview of the three main types of bone destruction patterns with representative image examples.
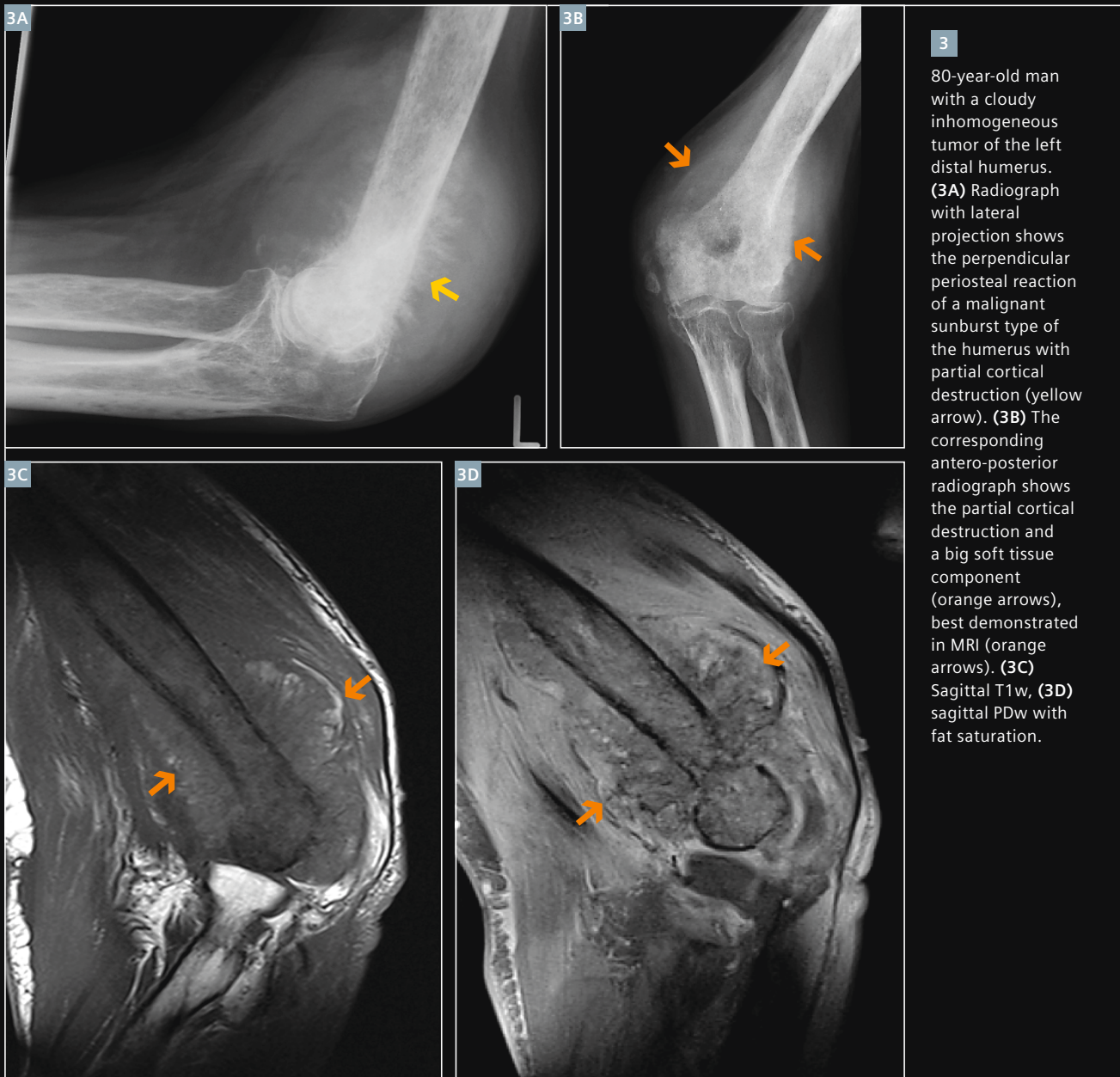
## Criteria of malignancy (Fig. 3)

Periosteal reactions are also indicators of lesion aggressiveness and can be differentiated according to a benign (thick, dense, wavy) type or an aggressive (lamellated, amorphous, sunburst) type. Figures 3A–D show an example of an 80-year-old man with a cloudy inhomogeneous tumor of the distal humerus with perpendicular periosteal reaction of a malignant sunburst type, partial cortical destruction and a big soft tissue component, best seen in MRI. All these criteria suggest a malignant process. Differential diagnoses are osteosarcoma or bone metastasis. Biopsy results in the diagnosis of metastasis of rectal cancer (adenocarcinoma).

## Types of bone tumors

According to their type of matrix (osteolytic, osteoblastic, or osteolytic with matrix mineralization) and to their tissue of origin, bone tumors are categorized into different types: osteoid, chondroid, fibrous, lipoid/fatty, other, cystic (solitary bone cyst, aneurysmal bone cyst), vascular (hemangioma), special cell type: Giant cell (osteoclastoma), small cell (Ewing's sarcoma), histiocytes (eosinophilic granuloma), plasma cells (multiple myeloma), notochordal cells (chordoma) and metastases.

**3** 80-year-old man with a cloudy inhomogeneous tumor of the left distal humerus. **(3A)** Radiograph with lateral projection shows the perpendicular periosteal reaction of a malignant sunburst type of the humerus with partial cortical destruction (yellow arrow). **(3B)** The corresponding antero-posterior radiograph shows the partial cortical destruction and a big soft tissue component (orange arrows), best demonstrated in MRI (orange arrows). **(3C)** Sagittal T1w, **(3D)** sagittal PDw with fat saturation.

# Osteoid type

### Osteoid osteoma and Osteoblastoma (Fig. 4)

This entity is frequent: around 13.5% of all benign bone tumors are osteoid osteomas. The patients are usually younger than 30 years and suffer „night pain relieved by aspirin" and other platelet aggregation inhibitors. The main location is in more than 50% within diaphysis of long bones and in 10% within the vertebral column with painful scoliosis. Osteoid osteomas show in CT and X-ray a perifocal sclerotic lesion with a central lucency (nidus) that is cortically based in 80%. Medullary, subperiosteal and articular locations also occur. Calcification of

the nidus is possible. The nidus is extremely vascular in contrast-enhanced MRI and it is important to identify the nidus as the tumor itself; surrounding sclerosis and bone marrow edema pattern is just reactive. It should be noted that lesions may have less or no sclerosis if the nidus is located in the marrow or in/adjacent to a joint (Fig. 5). Osteoid osteoma resembles osteomyelitis: For example if a Brodie's abscess is in an eccentric position, e.g. cortically located, it is difficult to differ Brodie's abscess from osteoid osteoma. The differentiation can then only be done by biopsy or radionuclide bone scan:

Osteoid osteoma shows – in contrast to osteomyelitis – the 'double density sign' (i.e. a high intense central activity surrounded by an area of medium activity). A lesion larger than 1.5 cm is called osteoblastoma [7, 11]. Radiofrequency ablation (RFA) is a successful treatment [8, 9, 10].

Keys to diagnosis: Sclerotic lesion with a small lucency in X-ray. The nidus shows a high signal on T2-weighted MR images and has a strong contrast-enhancement.
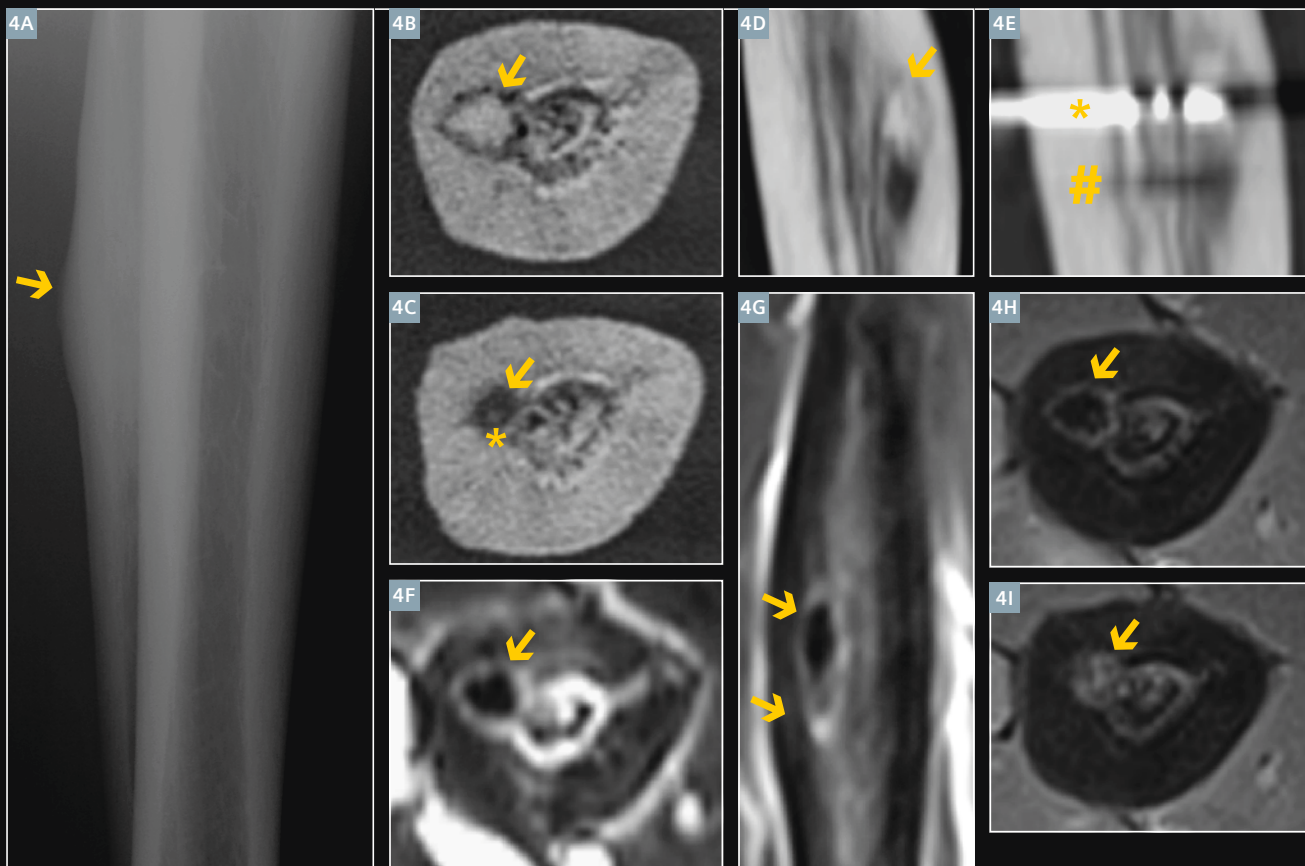


**4** 16-year-old male patient with osteoidblastoma (OB) of the right fibula. **(4A)** lateral radiograph shows well the cortical swelling of the fibula in the patient with OB but without lucency. The reason for that is best seen in **4B, C** (axial CT in different positions) and **4D** (coronal CT), where the upper part of the nidus is completely calcified whereas the smaller lower part shows only little calcification (*). **(4E)** shows a coronal CT with the ablation cannula (*) in the upper calcified part of the nidus during CT-guided radiofrequency ablation and the second ablation channel thereunder (#). T2w STIR images (**4F** axial and **4G** coronal) as well as T1w axial images **(4H, I)** demonstrate the vascularisation of the lower and the calcification of the upper nidus part with low T2w signal.
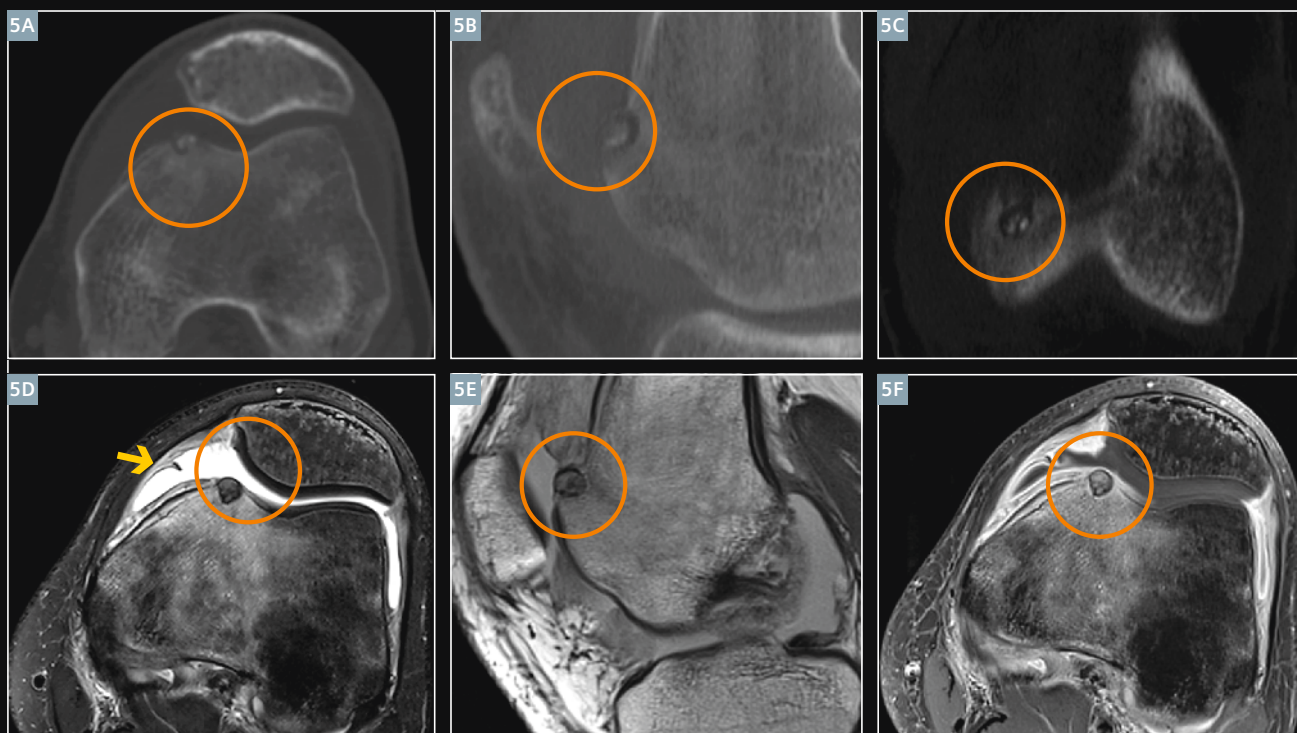
**5** 17-year-old male patient with articular osteoid osteoma (OO) of the left knee joint. **(5A–C)** Axial, sagittal and coronal CT with the articular position of the OO show no sclerosis of the nidus-margin (orange circle). In CT you see well that the nidus shows some central ossifications. The axial T2w MRI with fat saturation **(5D)** demonstrates the joint effusion and synovitis (yellow arrow). You can also see well that because of the central nidus calcifications the OO has only isointense to less hyperintense signal in T2w (orange circle) instead of the typical strong hyperintense signal. **(5E)** Sagittal PDw MRI also shows the calcification. **(5F)** Axial contrast-enhanced T1w MRI with fat saturation demonstrates the enhancing nidus (orange circle).
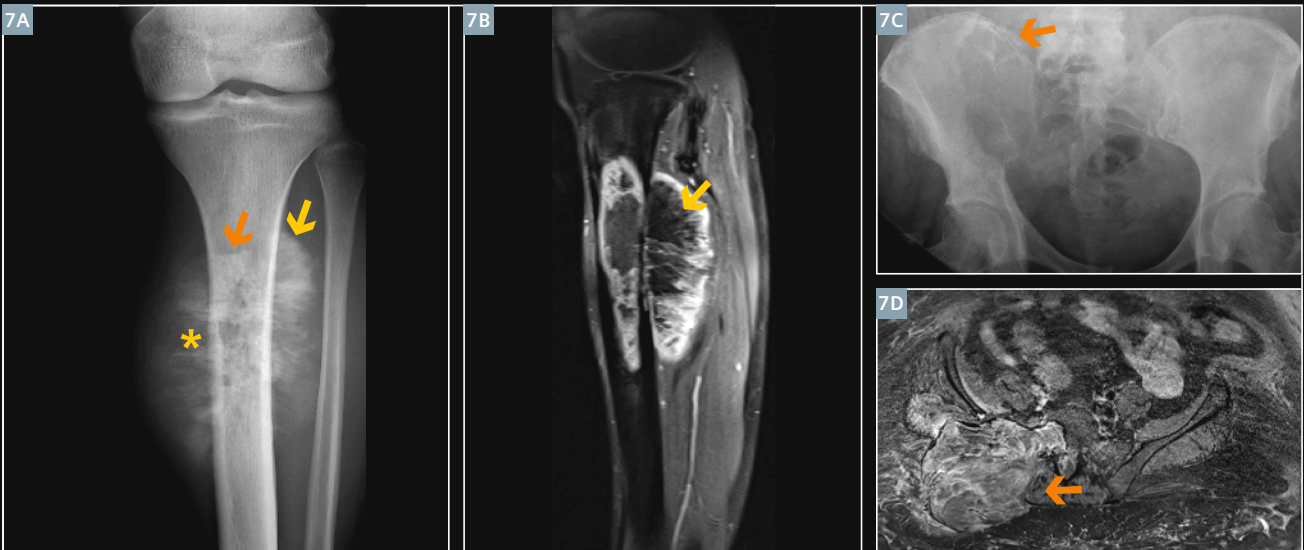
## Osteosarcoma

The patients are usually younger than 20 years. A 2nd peak exists in the 5th decade and these cases are mostly secondary in Paget's disease and after irradiation. Osteosarcoma has a predilection for sites of rapid bone growth, usually the metaphyseal region. Typical symptoms are pain and local swelling. This entity shows typically destructive periosteal reactions as mentioned above (Fig. 6). Their X-ray morphology is very variable: Osteosarcomas may be osteogenic (i.e. the tumor induces new bone formation), lytic or mixed, which is the common manifestation form (Fig. 7) [12]. If such a lesion is lytic, consider also teleangiectatic osteosarcoma! From origin, sclerosis grade and soft tissue component, osteosarcomas are separated into a central, parosteal (originates from the periosteum) and a periosteal variant, which is very rare (1% of osteosarcomas). In periosteal osteosarcomas the process starts either in the periosteum or adjacent soft tissue. Typical – in contrast to parosteal osteosarcoma – the periosteal osteogenic sarcoma does not have large amounts of calcification in the soft tissue (Fig. 8) [11]. Osteosarcomas may produce osteoblastic lung metastases (Fig. 9).

Keys to diagnosis are to detect criteria of malignancy in X-ray and further imaging modalities: CT is the best for identifying periosteal reaction versus tumor matrix because you can already see faint mineralization in CT. In MRI the signal depends on the degree of matrix mineralization. But MRI is important for assessing the tumor extent and for staging purposes, i.e. to identify skip-lesions, to assess the soft tissue, nerve and vessel involvement, and a potential joint infiltration.
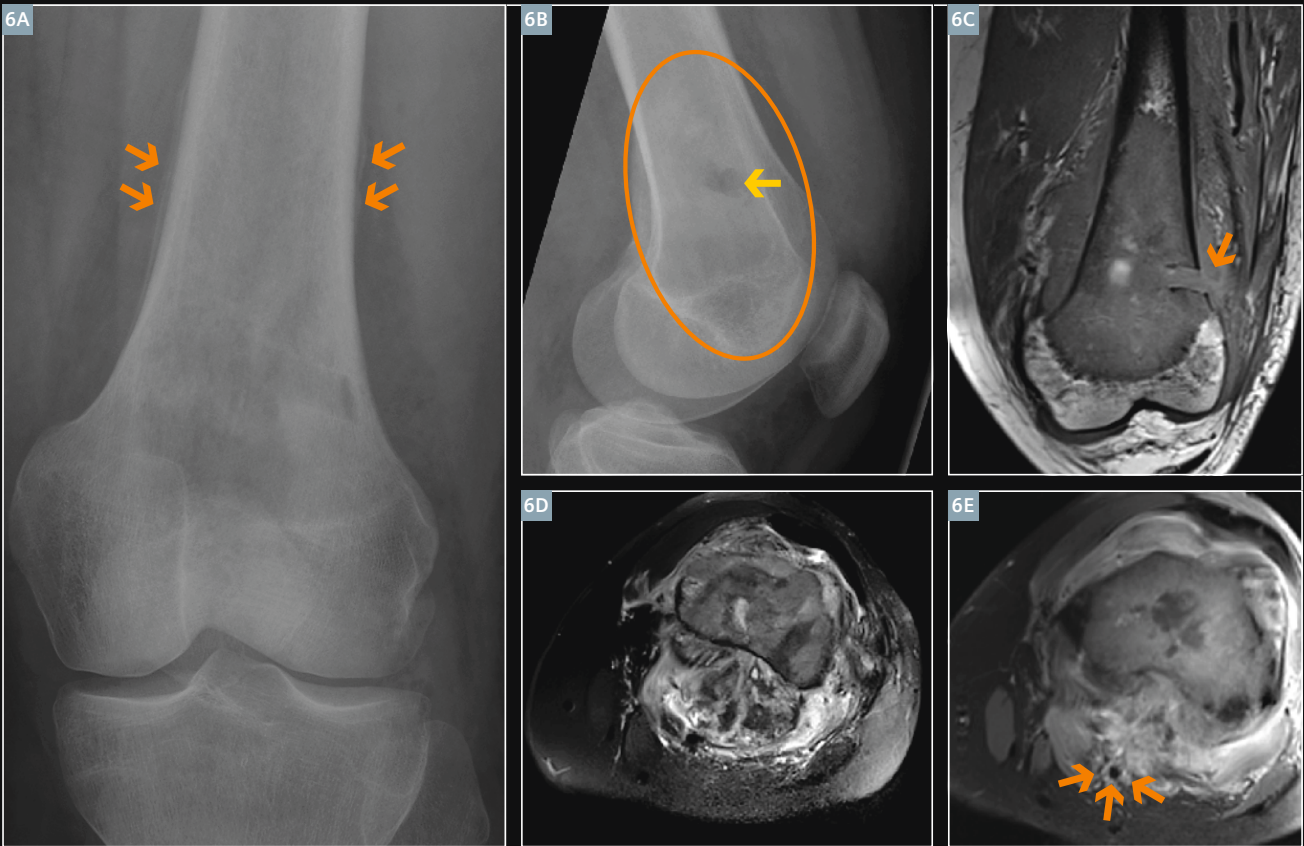
**6** 21-year-old man with a central high-grade osteosarcoma in the distal left femur. Conventional osteosarcomas are the central osteosarcomas placed in the center of the metaphysis. Figure **(6A)** shows the antero-posterior and **(6B)** the lateral radiograph. In this case you can see in addition to periosteal reactions (orange arrows in 6A) the channel-shaped lucency in the radiograph correlating with the biopsy channel (yellow arrow in 6B) within a disorganization of the bone pattern and osteoid formation (orange circle in 6B). You also see the biopsy channel in the coronal T1-weighted MRI (orange arrow in **6C**). Figure **6D** demonstrates the heterogeneity of the tumor mass (axial T2w MRI with fat saturation). Performing MRI is important for preoperative local staging, e.g. in this case the vessel infiltration (orange arrows in **6E**) is visible in the axial post-contrast T1-weighted MRI.

**7** These images demonstrate well the difference between osteogenic versus lytic osteosarcoma. Figures **7A** (antero-posterior radiograph of the lower leg) and **7B** (sagittal contrast-enhanced T1w MRI with fat saturation of the lower leg) show an osteogenic parosteal osteosarcoma of the left tibia, a bone forming tumor with fluffy, amorphous, cloudlike mineralization (orange arrow in 7A) beside sunburst periosteal reaction as a criterion of malignancy (* in 7A). This tumor has a big soft tissue component (yellow arrow in 7B) with large amounts of calcification (yellow arrow in 7A). Figures **7C** (antero-posterior radiograph of the pelvis) and **7D** (axial contrast-enhanced T1w MRI with fat saturation) show a more lytic osteosarcoma of a 61-year-old female patient in the right os ileum with no mineralization (orange arrow).
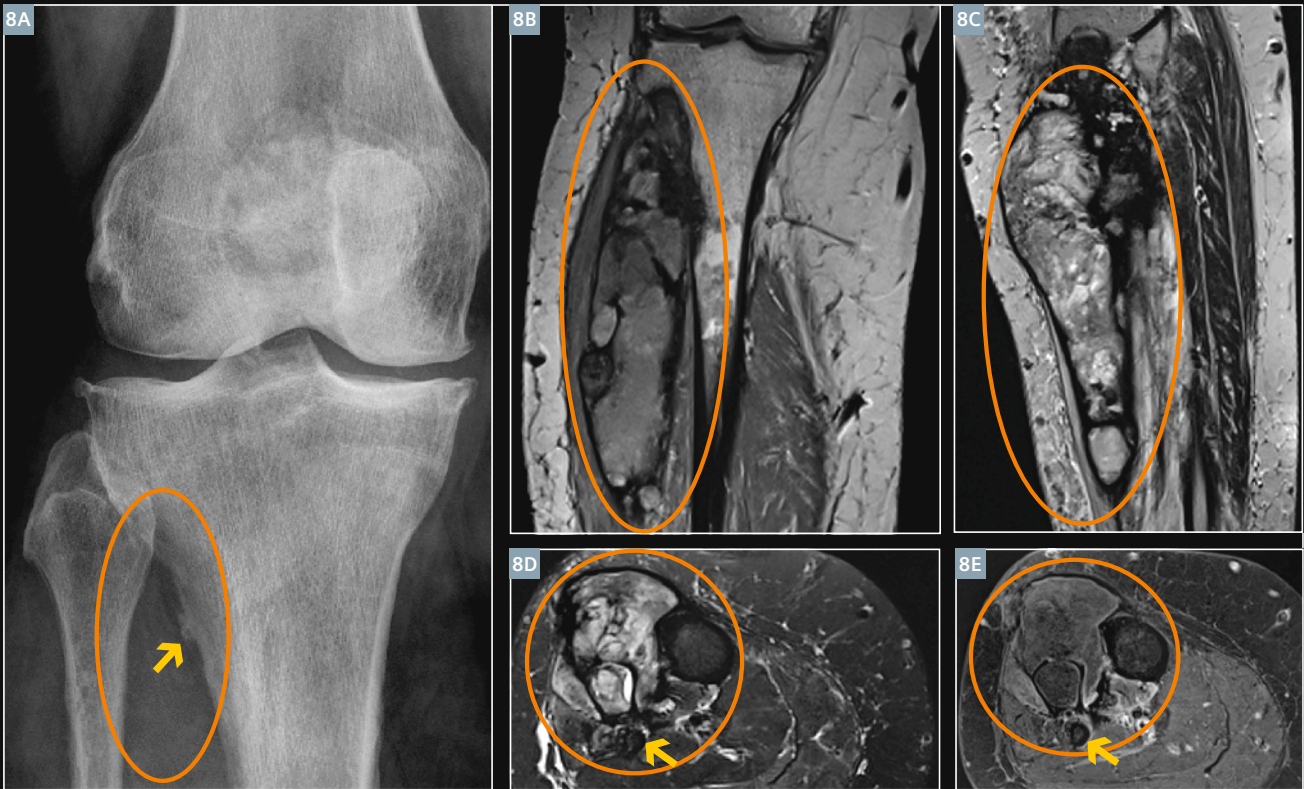
**8** 57-year-old female patient with a periosteal osteosarcoma (G3) of the right lower leg. Figure **8A**, antero-posterior radiograph of the right knee shows saucerization of the tibial metaphysic (orange circle) and also a bone prominence (yellow arrow). **8B** (coronal T1w MRI of the lower right leg) and **8C** (sagittal T1w MRI of the lower right leg) show the big inhomogeneous tumor with a large soft tissue component. Keep in mind that the periosteal osteogenic sarcoma does not have large amounts of calcification in soft tissue as shown in 8A–C (orange circle). Figures **8D** (axial T2w MRI with fat saturation) and **8E** (axial contrast-enhanced T1w MRI with fat saturation) clearly demonstrate that the tumor inexplicably will not invade the medullary space of the tibia (orange circle) and that the fibula is not involved (yellow arrow).
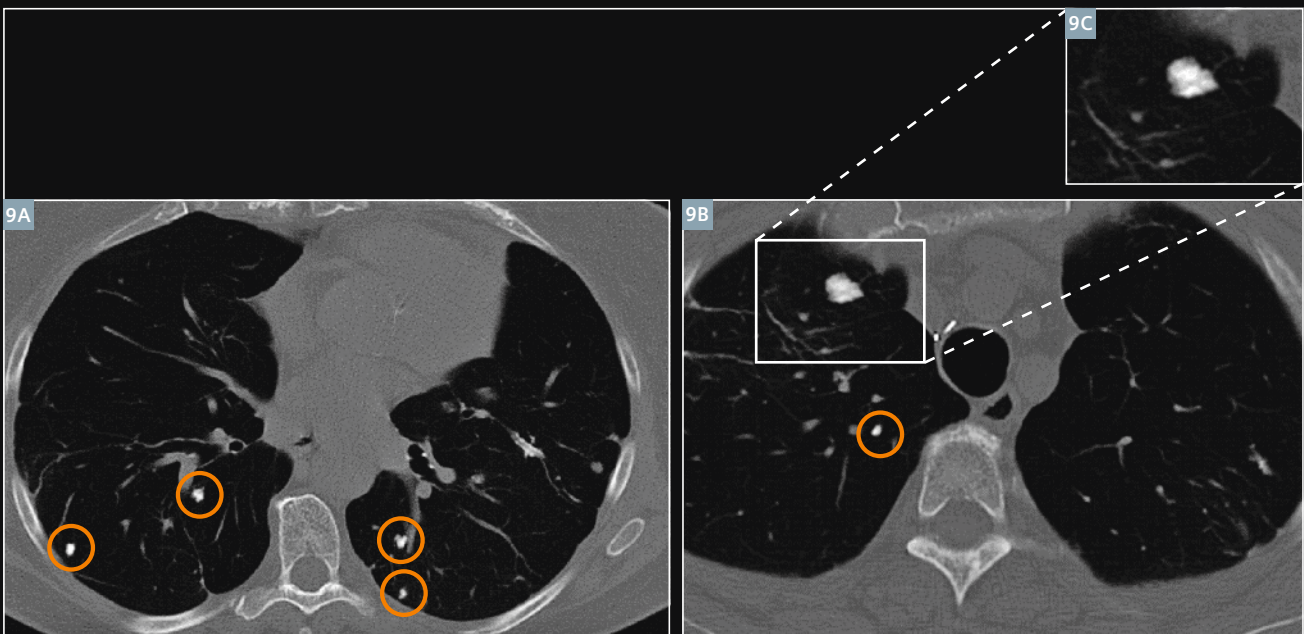


**9** 63-year-old female with osteoblastic lung metastases one year after resection of an osteosarcoma of the left thigh. Axial CT images **(9A–C)** show several osteoblastic lung metastases of a bone producing primary tumor: an osteosarcoma. Therefore the lung metastases may be also sclerotic.

# Chondroid type

### Enchondroma

Enchondroma is a benign lytic lesion typically placed in the hand and chiefly centrally located, often with endosteal scalloping. It must have calcification except in the phalanges (Fig. 10). A typical size of enchondroma is around 1–2 cm; low grade chondrosarcoma is larger than 4–5 cm. The enchondroma shows no periosteal reaction. An important differential diagnosis is the bone infarction (Fig. 12).

Keys to diagnosis are: In T1-weighted MR imaging the lesion has a low signal. The T2-weighted signal depends on the degree of calcification. After contrast-enhancement the tumor shows in T1-weighting MR imaging a lobulated appearance with septa (Figs. 10 and 11).

Suspicious of malignancy in chondroid tumors are pain, a size larger than 5 cm, the presence of a soft tissue mass and a growing surrounding edema on T2-weighted images.

Multiple enchondromas occur on occasion, a condition called Ollier's disease. This is not hereditary and with no increased rate of malignant degeneration.

By contrast, Maffucci's syndrome is a condition with multiple enchondromas associated with soft tissue hemangiomas. Maffucci's syndrome is likewise not hereditary, but is characterized by an increased incidence of malignant degeneration of the enchondromas [11].
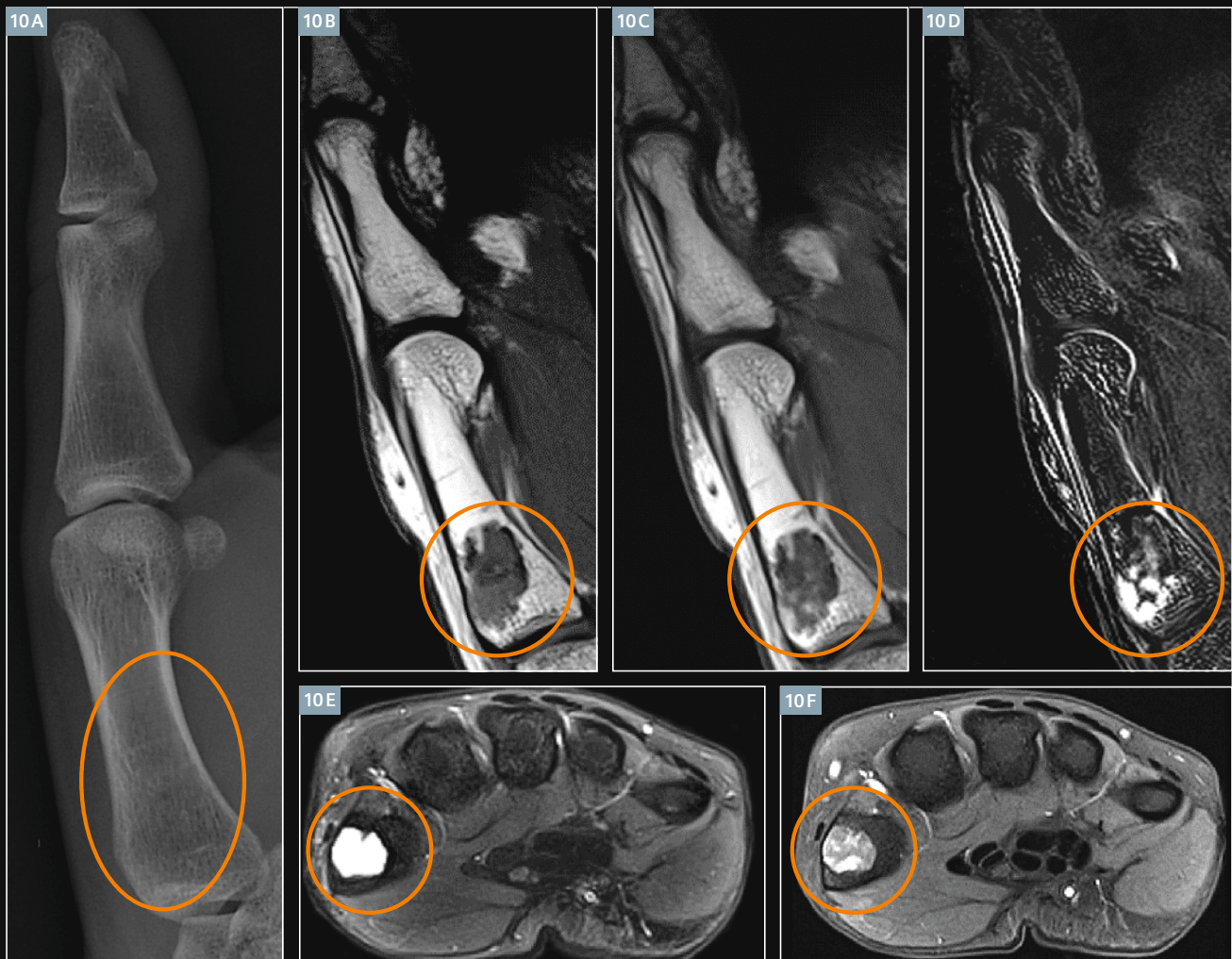


**10** 29-year-old female with an enchondroma of the phalanx D1. **(10A)** Lateral radiograph of the right D1 shows the lytic lesion in the proximal metacarpus of D1 which is hardly to identify and without sclerotic rim, according to a Lodwick IB lesion (orange circle) and without calcifications. (10B-F) show the typical signal characteristics of an enchondroma in MRI (orange circles) and that the lesion is smaller than 2 cm: low signal in T1-weighted imaging (**10B**, coronal), high signal in T2-weighted imaging because of absent calcification as shown in 10A (**10E**, axial T2w MRI with fat saturation). Coronal contrast-enhanced T1w MRI **(10C)**, coronal T1w MRI subtraction **(10D)**, and axial contrast-enhanced T1w MRI with fat saturation **(10F)**, show that the tumor has a lobulated appearance with septa.
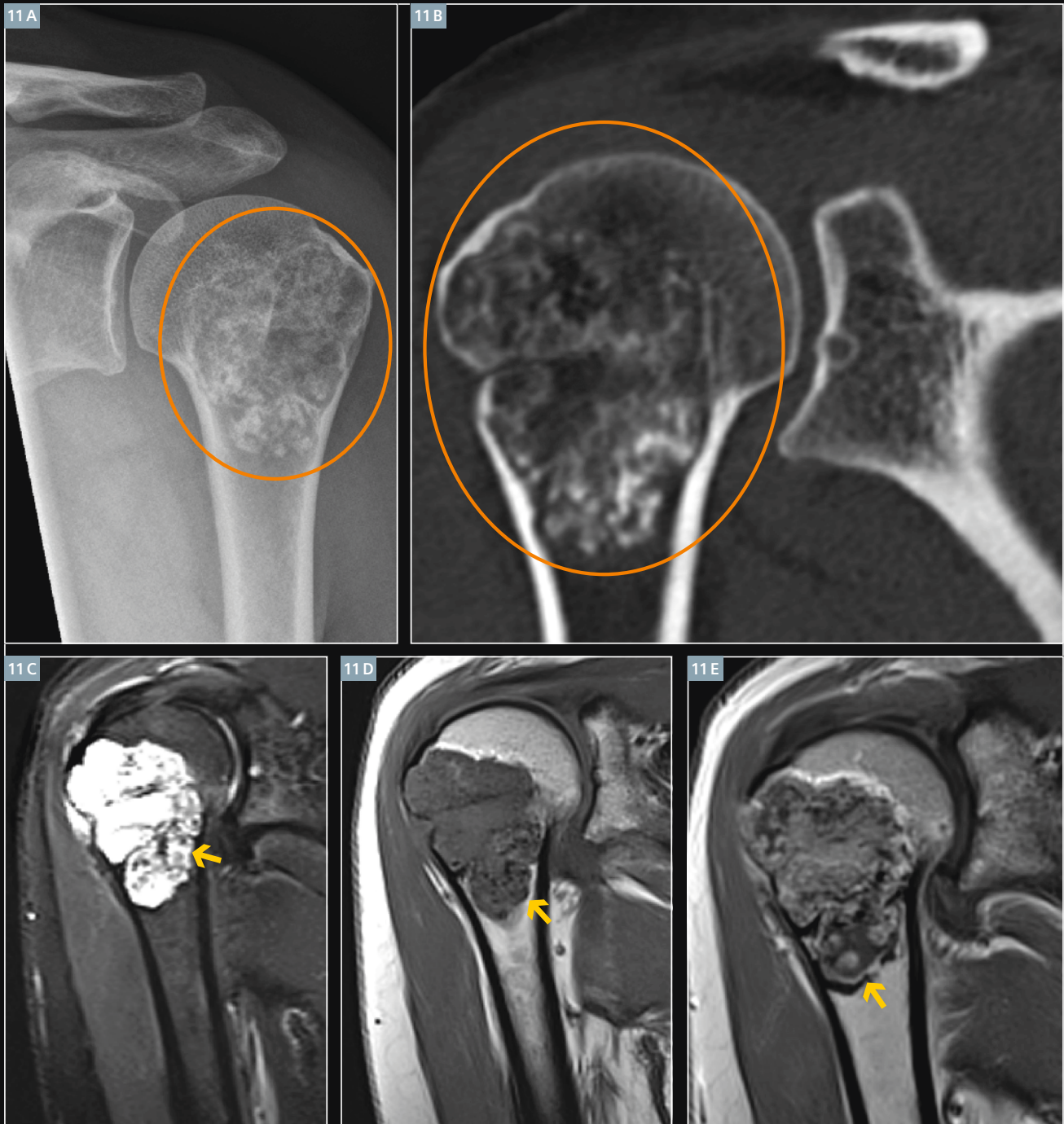
11    44-year-old female with an enchondroma within the humeral head. **(11A)** Antero-posterior radiograph of the shoulder, **(11B)** coronal CT of the shoulder, **(11C)** coronal T2w MRI with fat saturation, **(11D)** coronal T1w MRI, **(11E)** coronal contrast-enhanced T1w MRI. 11A and B show a lesion bigger than 2 cm with a sharp border (Lodwick IB) in the humerus head with the following different forms of calcification of the chondral tissue: Punctate, comma-shaped, arc like, ring like mineralization (orange circle). In T1w the tumor shows low signal **(11D)**, in T2w with fat saturation high signal with some low signals according to the calcifications, thus containing no fat **(11C)** and post-contrast a homogenous contrast-enhancement with a rough lobulated pattern **(11E)** (yellow arrows).
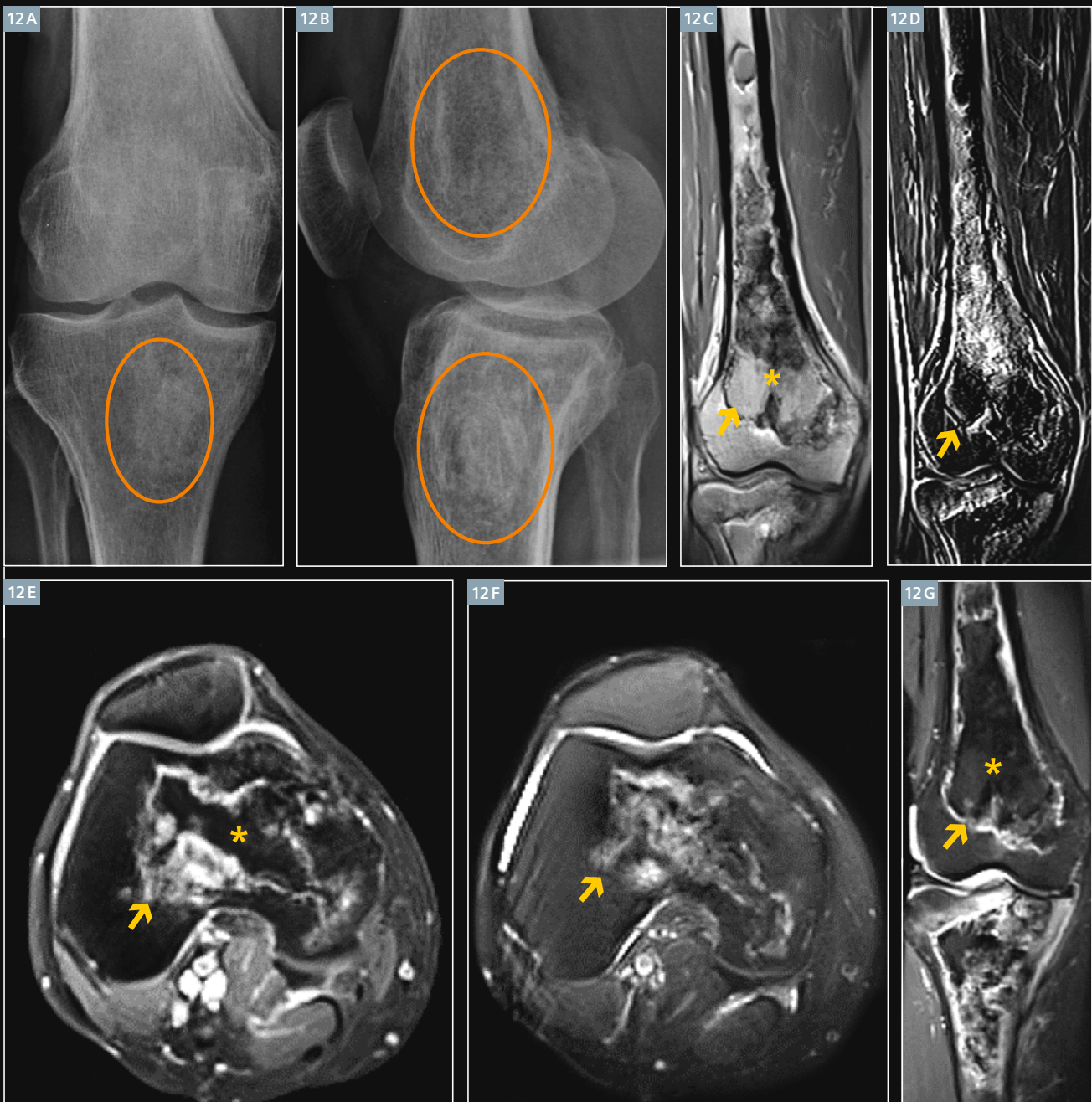
**12** 40-year-old female with bone infarction in the right tibia and femur. **(12A)** Antero-posterior, **(12B)** lateral radiograph of the knee, **(12C)** coronal contrast-enhanced T1w MRI, **(12D)** coronal T1w subtraction MRI, **(12E)** axial contrast-enhanced T1w MRI with fat saturation, **(12F)** axial T2w MRI with fat saturation, **(12G)** coronal STIR MRI. An infarct usually has a well-defined, densely sclerotic, serpiginous border as well shown in 12A and B (orange circles) and in MRI in 12C-G (yellow arrow), whereas an enchondroma does not. Fat in the lesion as seen in 12C, E and G (yellow star) is a hint of bone infarction and speaks against an enchondroma.

## Chondroid type

### Osteochondroma (Fig. 13)

A synonym for osteochondroma is cartilaginous exostosis. It is a common benign tumor of the extremities (10%–15% of all bone tumors) and is located in 50% of cases in the lower extremities, in 10–20% in the humerus, but rarely in the spine. For the diagnosis it is important to identify the con-tinuation of bone marrow and trabecular bone structures into the exostosis as well as the cartilage cap. The malignant degeneration occurs mainly in tumors near the trunk.

Key to diagnosis is a mushroom-like tumor. The thickness of the cartilage cap is 8 mm or more (threshold in our institution, see also explanation in the next chapter) (Fig. 13) [13]. Contrast media is not needed to determine the thickness of the cartilage cap, because it is clearly visible on T2-weighted images.
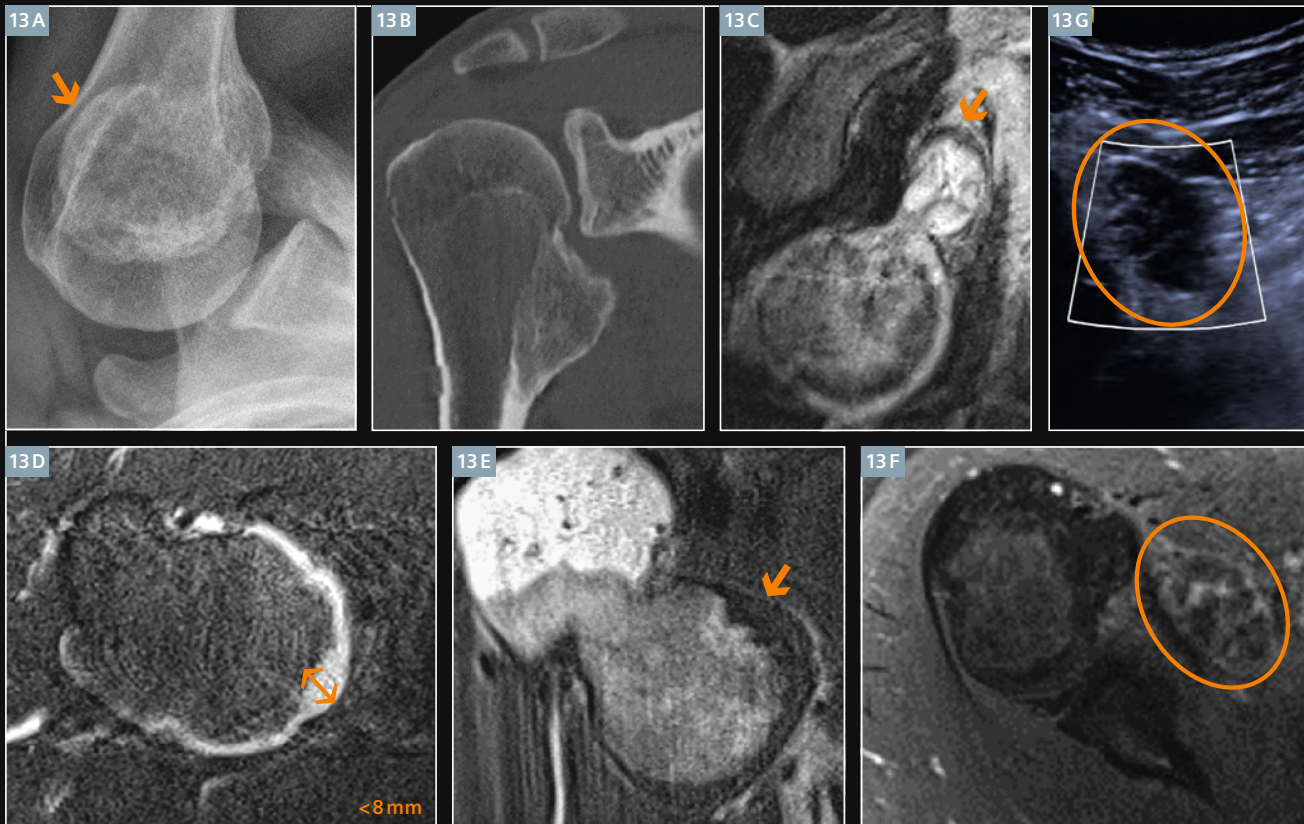


**13** 20-year-old male patient with an osteochondroma of the proximal right humerus and a loose body within joint space. **(13A)** Axial radiograph of the right shoulder shows the sharp-bordered tumor of the humerus, **(13B)** coronal CT shows the osteochondroma of the right shoulder, **(13C)** sagittal T2w MRI shows another part of the osteochondroma with its cartilage cap, where the cap seems to be much larger than 8 mm, see also 13F, **(13D)** axial T2w MRI with fat saturation shows the measurement of the T2w hyperintense cartilage cap with a distance of 8 mm, **(13E)** coronal T1w MRI shows the cartilage cap that is hypointense in T1w, **(13F)** axial contrast-enhanced T1w MRI with fat saturation show the same part of figure 13C with a chondroid lobated pattern after contrast-enhancement, **(13G)** 9 MHz ultrasound shows the structure seen in 13C and G as a round non-cystic structure. This lesion is with all imaging modalities suspicious of a low grade chondrosarcoma. After surgery and histologic examination revealed it to be no more than an osteochondroma and a neighboring loose body within joint space with caplike borders and nodose lobulated chondroid tissue with kept structure of the lobules.

## Osteochondroma
## vs. chondrosarcoma

A malignant transformation is more likely if the cartilage cap thickness is 8 mm or more, which is the threshold of our clinic. Further publicized threshold values are 1.5 cm according to Murphey et al. [14] and 2.0 cm according to Bernard et al. [15]. Proximity to trunk (location in the pelvis with highest malignant transformation rate!) and hereditary multiple exostoses (autosomal dominant inheritance) (Fig. 14) are correlated with a higher risk of malignant transformation (3–5% of tumors develop into chondrosarcomas). A further criterion is a cartilage cap growth, especially beyond age 20. Note: It is extremely difficult for either a radiologist or a pathologist to differentiate a low-grade chondrosarcoma from enchondroma (Fig. 15).



**14** 12-year-old male patient with hereditary multiple exostoses. **(14A)** Axial radiograph of the left shoulder, **(14B)** antero-posterior radiograph of the left shoulder, **(14C)** axial T2w MRI with fat saturation of the left humerus, **(14D)** sagittal T2w MRI with fat saturation of the left humerus, **(14E)** lateral radiograph of the left knee, **(14F)** antero-posterior radiograph of the left knee, **(14G)** coronal STIR MRI of the upper extremities. In 14A, B, E and F the continuation of bone marrow and trabecular bone structures into the exostosis are clearly depicted. The cartilage cap can be well evaluated in T2-weighted images as seen in 14C, D and also in 14G.

### Chondrosarcoma (Figs. 15–17)

Patients are mostly older than 40 years and experience pain. Tumors are near the trunk and have a chondroid matrix. Chondrosarcomas are characterized by slow growth. Primary chondrosarcomas are lytic, permeative and destructive lesions with calcification in 50%. Secondary chondrosarcomas have a cartilage cap's thickness larger than 8 mm as a sign of malignant transformation of an osteochondroma (see also the comments to threshold value in the last chapter) [13-15].

Keys to diagnosis are lytic, destructive lesion with flocculent, snowflake or popcorn calcification in patients older than 40 years. MRI: soft tissue mass or edema. The following criteria are in favor of a chondrosarcoma as opposed to an enchondroma: Pain, tracer uptake in bone scan, growth, cortical bone penetration.
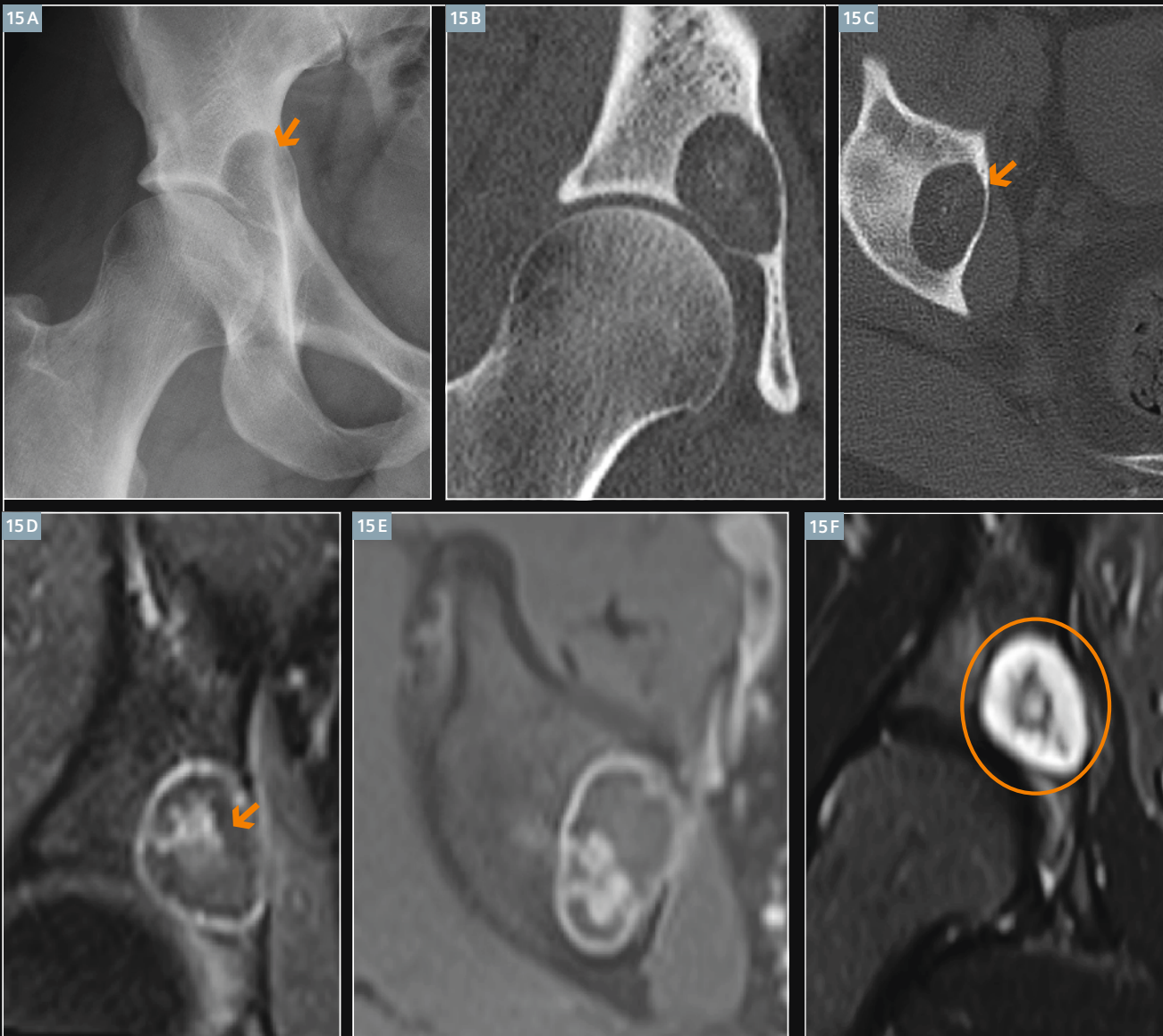
**15** 31-year-old male patient with grade 1 chondrosarcoma of the right os ilium. **(15A)** The antero- posterior radiograph of the right hip joint shows a geographic well-defined lytic lesion in the right acetabulum with a sharp border but without sclerotic rim according to a Lodwick IB lesion (orange arrow), in the center there is some flocculent calcification. **(15B)** Coronal CT and **(15C)** axial CT of the right hip show the lytic lesion with sharp border, thinned cortex and central punctuate calcification without cortical destruction. **(15D, E)** Contrast-enhanced T1w MRI with fat saturation (coronal in 15D and axial in 15E) show a central contrast-enhancement. Figure 15F shows a coronal STIR MRI with a high signal in the border area of the tumor.
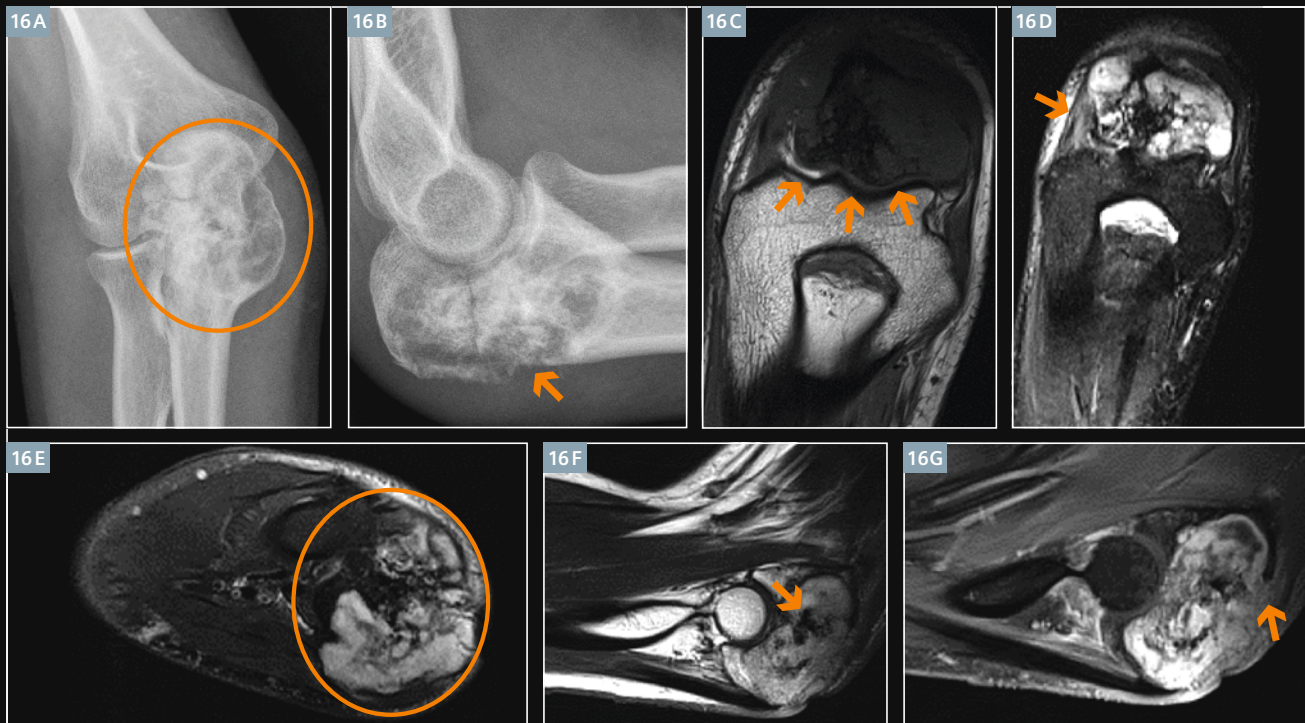
**16** 33-year-old female with grade 2 chondrosarcoma of the left olecranon. **16A** shows an antero-posterior radiograph of the left olecranon with a Lodwick type IC lesion: geographic but blurred border (orange circle). Figure **16B** shows the lateral radiograph of the left olecranon and reveals a cortical destruction (orange arrow). **(16C)** Coronal T1-weighted MR image of the olecranon clearly shows the intraosseous borders of the tumor (orange arrows). **(16D)** Coronal STIR MR image clearly shows the muscle edema (orange arrow). **(16E)** Axial T2w MRI with fat saturation shows the chondroid matrix of the tumor (orange circle). **(16F)** Sagittal T2w MRI shows the hypointense calcification (orange arrow) in the center of the chondroid tumor. **(16G)** Sagittal contrast-enhanced T1w MRI with fat saturation shows the infiltration of the surrounding soft tissue (orange arrow).
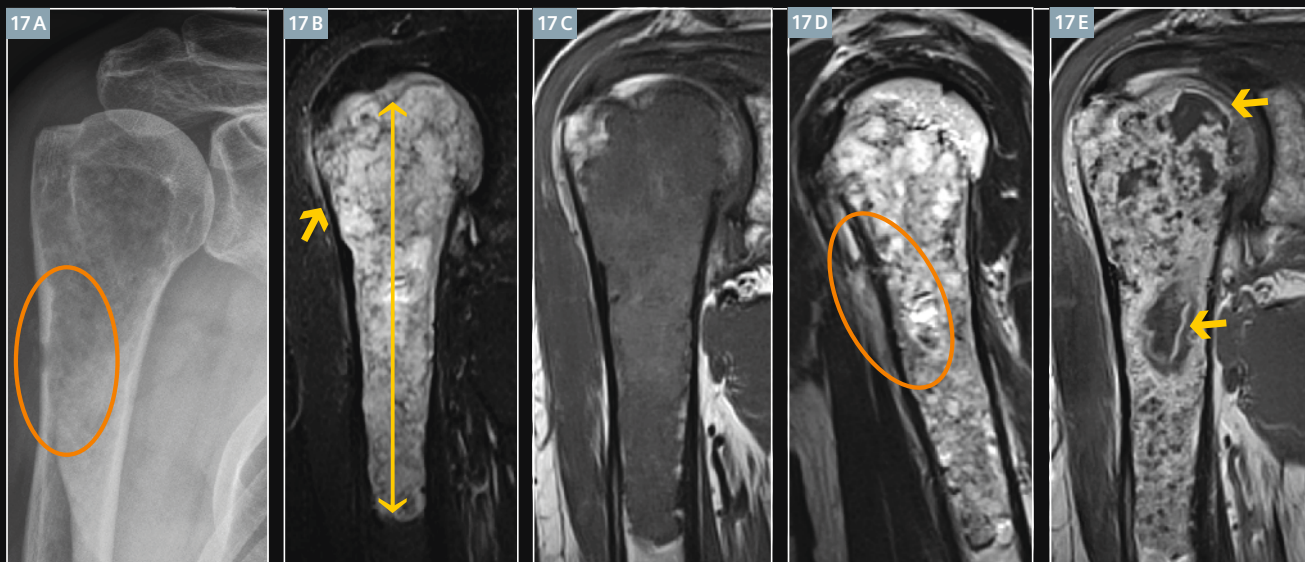


**17** 58-year-old male patient with grade 3 chondrosarcoma of the right humerus. **(17A)** The antero-posterior radiograph of the right humerus shows in addition to a patchy lysis pattern (Lodwick II) the cortex destruction (orange circle). **(17B)** Coronal STIR MRI clearly shows the extension of this large amorphous lesion (size of 10 cm, long yellow arrow) and the soft tissue infiltration (small yellow arrow). The tumor has a predominant chondroid matrix with low signal in T1w (**17C** coronal T1w MRI) and an inhomogeneous high signal in T2w (**17D** sagittal T2w MRI) as a further hint of a high-grade chondrosarcoma. (17D) Also shows well the cortex destruction and soft tissue infiltration (orange circle). **(17E)** Coronal contrast-enhanced MRI shows necrotic tumor areas within the tumor (yellow arrows). Also areas without chondroid matrix are a hint of a high-grade chondrosarcoma.
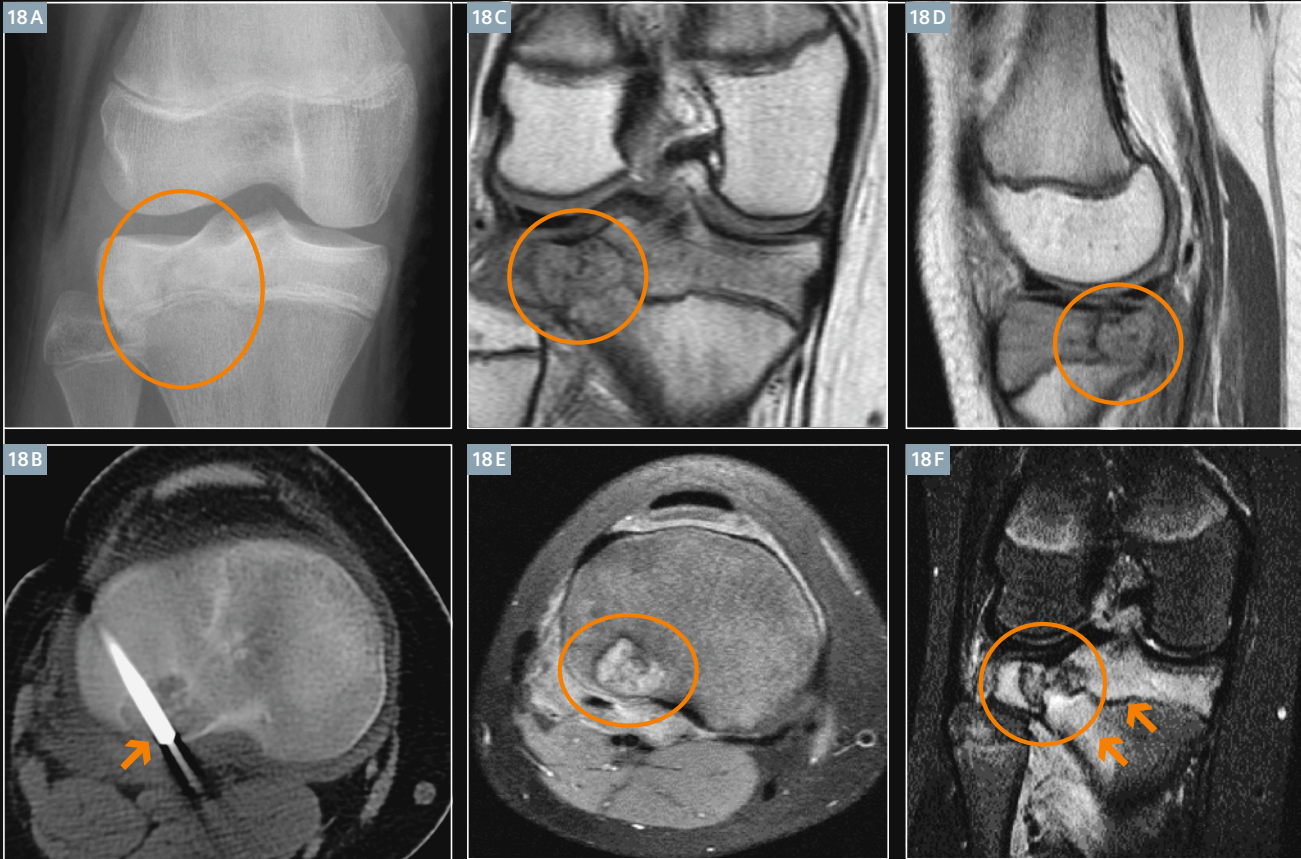
## Chondroblastoma (Fig. 18)

Patients are usually younger than 20 years (i. e. skeletally immature patients). The lesion must be located epiphyseally and is rare in metaphysis. This entity also occurs in carpal and tarsal bones and rarely in the patella (which with regard to the differential diagnosis of lytic lesions behaves like an epiphysis) [11]. Usually it appears in long bones and shows in 40–60% calcification. Differential diagnoses are the sequestrum (osteomyelitis) and the eosinophilic granuloma.

Key to diagnosis: Chondroblastomas are lytic epiphyseal lesions with sclerotic rim. In MRI it shows a chondroid component with high signal in T2-weighted imaging and calcification with low signal in T2-weighted imaging [4].



**18** 12-year-old female patient with a chondroblastoma of the right lateral tibia epiphysis. **(18A)** Antero-posterior radiograph of the right knee shows the epiphyseal located lytic lesion of the tibia with discreet sclerotic rim and some central located calcification (orange circle). **(18B)** Axial CT shows the puncture needle in that lytic lesion having a sharp border (orange arrow). **(18C)** Coronal and **(18D)** sagittal T1-weighted MR images show the bordered lesion having a discreet hypointense sclerotic rim and a central hypointense punctual calcification (orange circle). **(18E)** Axial PD-weighted MR image shows a chondroid component with high signal and central calcification with low signal (orange circle). **(18F)** Coronal STIR MR image also shows a chondroid component with high signal and central calcification with low signal (orange circle) and a bone marrow edema in the circumference (orange arrows). Therefore biopsy was performed.
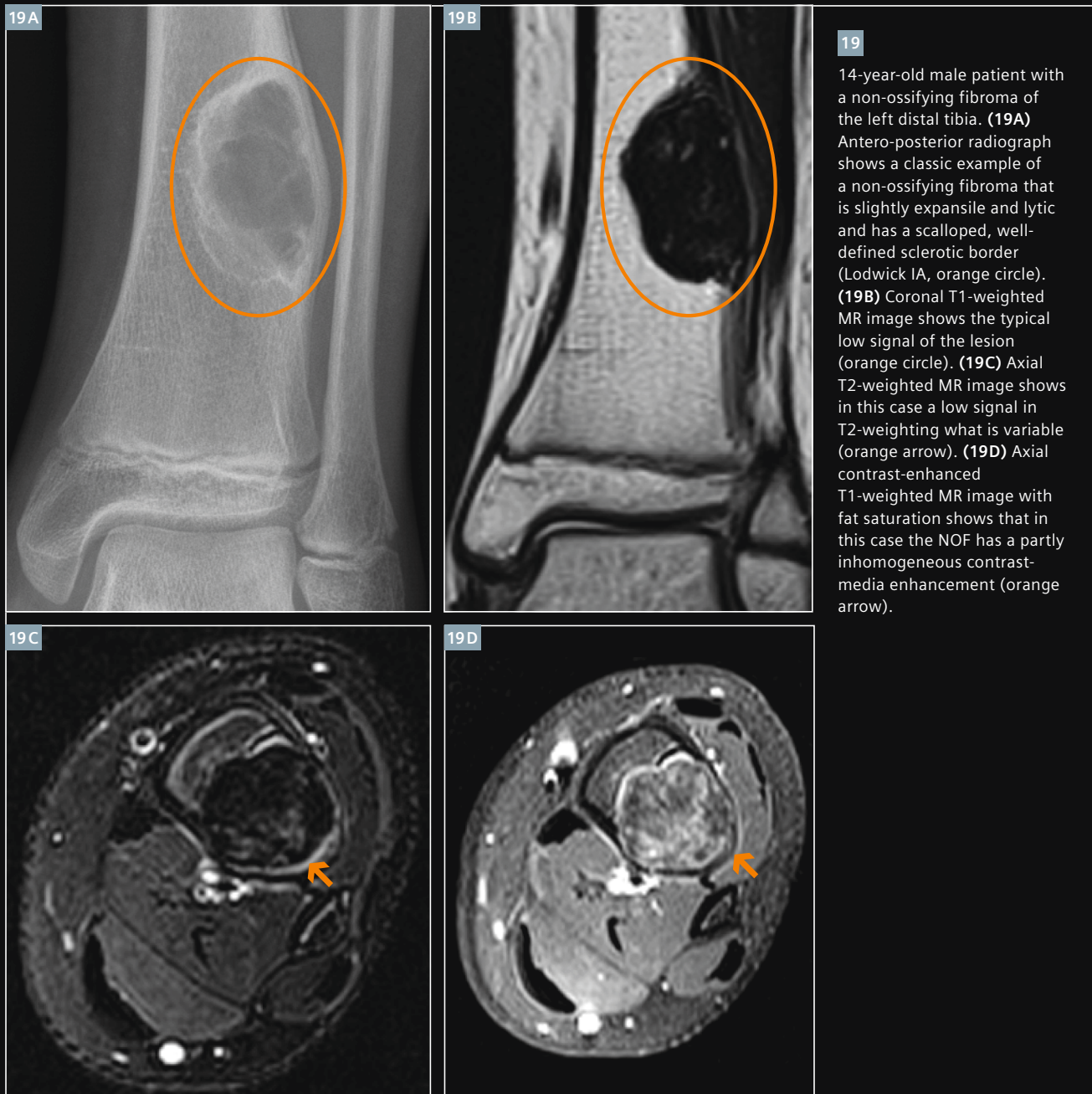
## Fibrous type

### Non-ossifying fibroma – NOF
### (Figs. 19 and 20)

Patients are usually younger than 20 years and have no pain or periosteal reaction. This lesion is located in the metaphysis of long bone in eccentric position and emanates from the cortex, so that the cortex will be replaced with benign fibrous tissue. Non-ossifying fibromas 'heal' with sclerosis and disappear in the following years. L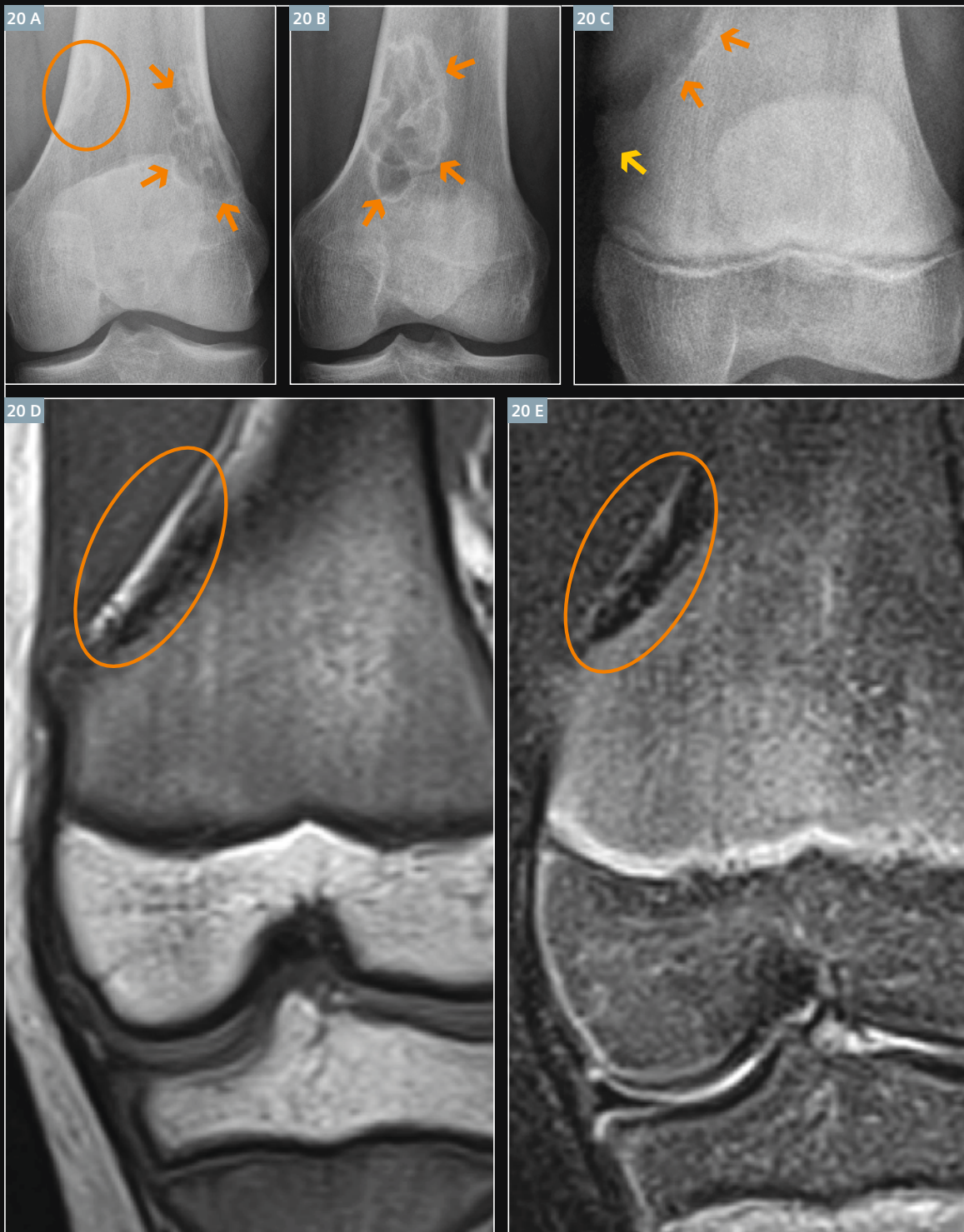esions smaller than 3 cm in length are called fibrous cortical defect and lesions larger than 3 cm in length are called non-ossifying fibroma.

Key to diagnosis: A lytic lesion with expansive growth and scalloped, well-defined sclerotic border. The MRI appearance of an NOF is somewhat variable. Although they are essentially always low signal on T1-weighted MR imaging, they can have high or low signal on T2-weighted imaging. NOF has partly homogeneous or partly non-homogeneous contrast-media enhancement. During the 'healing period' the non-ossifying fibroma can be hot on radionuclide bone scans indicating the osteoblastic activity.

**19**

14-year-old male patient with a non-ossifying fibroma of the left distal tibia. **(19A)** Antero-posterior radiograph shows a classic example of a non-ossifying fibroma that is slightly expansile and lytic and has a scalloped, well-defined sclerotic border (Lodwick IA, orange circle). **(19B)** Coronal T1-weighted MR image shows the typical low signal of the lesion (orange circle). **(19C)** Axial T2-weighted MR image shows in this case a low signal in T2-weighting what is variable (orange arrow). **(19D)** Axial contrast-enhanced T1-weighted MR image with fat saturation shows that in this case the NOF has a partly inhomogeneous contrast-media enhancement (orange arrow).

20  Image gallery of the non-ossifying fibroma.
(20A) Antero-posterior radiograph of the right knee of a 17-year-old male patient clearly shows the various appearance of a NOF. Two healing periods can be seen: Lateral, a lesion with proceeding sclerosis indicating that the lesion is in a progressed healing stadium (orange circle) and medial, a classical scalloped lesion with well-defined sclerotic border (orange arrows).
(20B) Antero-posterior radiograph of the left knee of an 18-year-old male patient shows the typical appearance of a NOF: Scalloped lesion with well-defined sclerotic border.
(20C) Antero-posterior radiograph of the knee of a 12-year-old male patient shows a lytic lesion with sclerotic rim (orange arrow) and below an exostosis (yellow arrow). (20D) Coronal T1-weighted MR image shows the typical low signal of a NOF (orange circle) and (20E) a coronal STIR MR image shows in this case also a low signal compatible to the diagnosis of a NOF.

## Fibrous dysplasia (Figs. 21–23)

Patients have usually no pain or periosteal reaction. Fibrous dysplasia can be either monostotic (most commonly) or polyostotic (McCune-Albright syndrome) and has a predilection for the pelvis, the proximal femur, the ribs and skull. In its classic description, fibrous dysplasia has a, 'ground-glass appearance' or 'smoky appearing' in X-ray and/or CT (Fig. 21), but the ground glass appearance is not always present. Lesions may be mixed lytic and sclerotic [11] and bone may be deformed.

Keys to diagnosis are: No periosteal reaction. Fibrous dysplasia shows lytic lesions, as the matrix calcifies it has a hazy, smoky and ground-glass look to the point of sclerotic lesion. The signal alterations of fibrous dysplasia in MRI follow the uniform pattern of all tumors (low signal in T1-weighted and intermediate to high signal in T2-weighted images). The fibrous tissue enhances contrast media. If the lesion is located in the tibia, consider also adamantinoma, which has malignant potential, i.e. a mixed lytic and sclerotic lesion in anterior cortex of tibia that resembles the fibrous dysplasia.
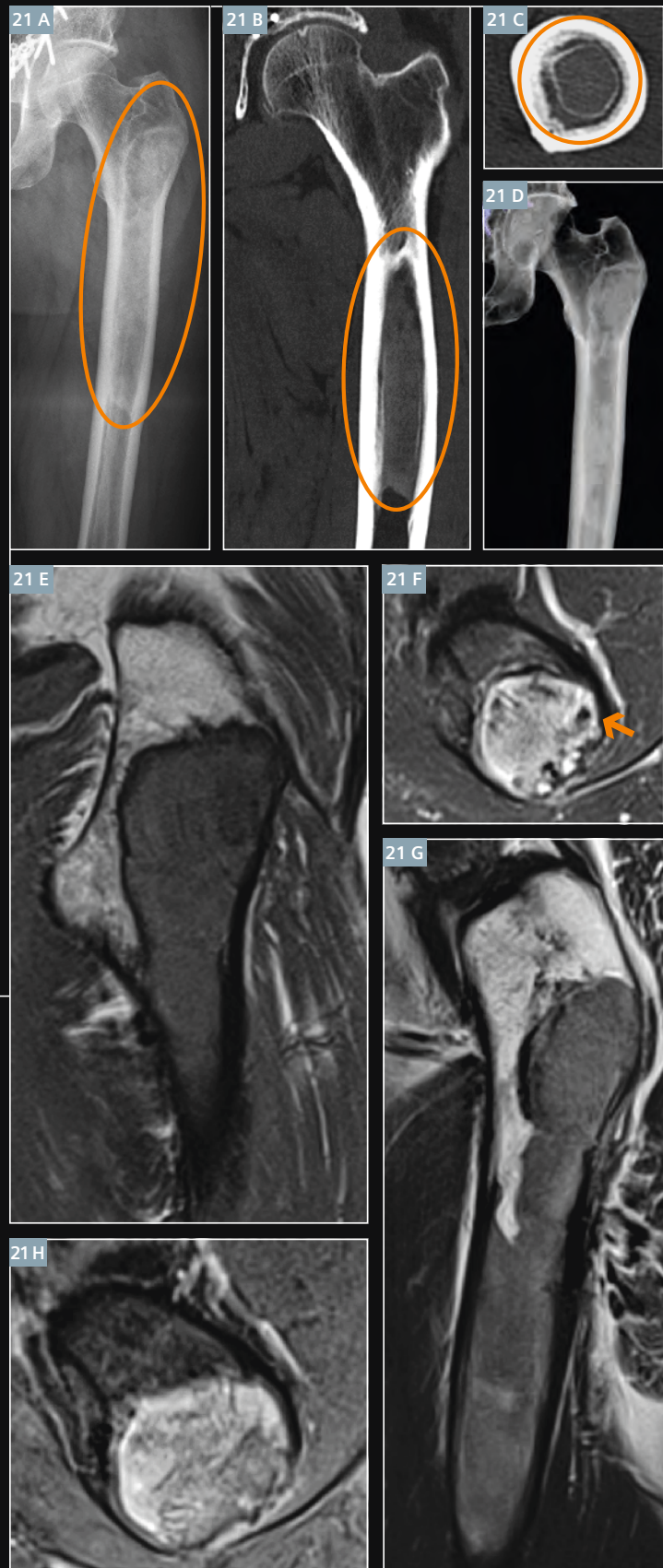


**21**

44-year-old male patient with fibrous dysplasia of the left femur.
**(21A)** Antero-posterior radiograph of the left femur shows well the ground glass appearance of a sclerotic lesion in the proximal diaphysis (orange circle). **(21B)** Coronal CT, **(21C)** axial CT and **(21D)** 3D figure also clearly show the ground glass appearance of that lesion (orange circle). **(21E)** Coronal T1-weighted MR image shows low signal of the lesion. **(21F)** Axial T2-weighted MR image with fat saturation shows that the lesion contains only point-shaped lipoid and calcified parts (orange arrow). **(21G)** Sagittal T2-weighted MR image shows in this case a homogenous low signal, **(21H)** axial contrast-enhanced T1-weighted MR image with fat saturation shows a relatively homogenous contrast enhancing of the lesion. An inhomogeneous contrast-enhancement occurs in lesions with bigger parts of blood, fat and calcifications leading to signal alterations.
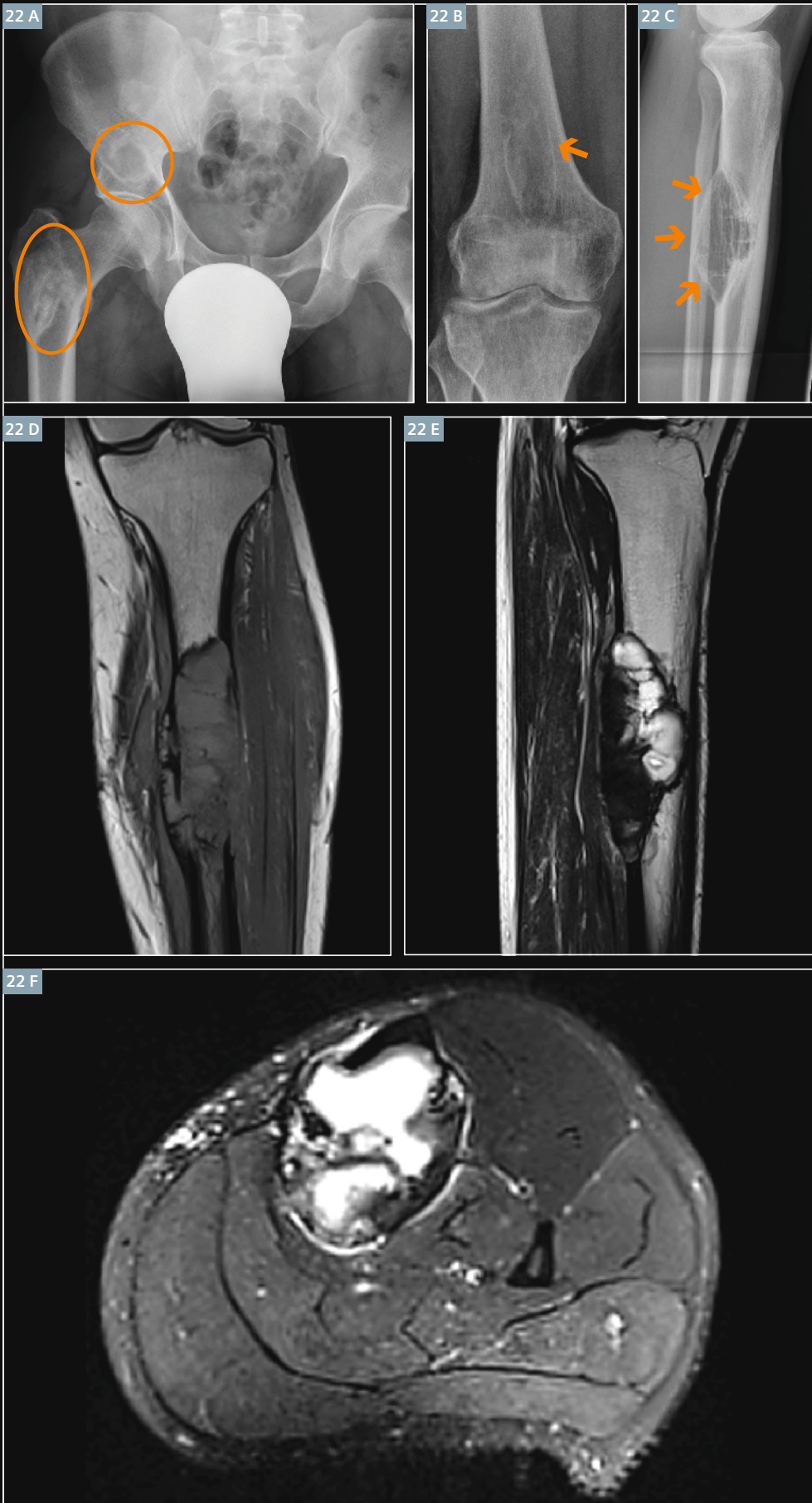
**22**

Image gallery of fibrous dysplasia: "Fibrous dysplasia...can look like almost anything!" [11], as is clearly visible when you compare the following three cases.
**(22A)** Antero-posterior radiograph of the pelvis of a 36-year-old male patient clearly shows that the ipsilateral proximal femur is always affected when the pelvis is involved with fibrous dysplasia (orange circles). The lesion in the pelvis is more lytic than the lesion in the femur which is more sclerotic. **(22B)** Antero-posterior radiograph of the right knee of a 33-year-old female patient shows a circumscripted lytic lesion of the distal femur with smoky parts (orange arrow). **(22C)** Lateral radiograph of the left lower leg of a 22-year-old male patient with a fibrous dysplasia of the tibia shows a lytic lesion in the tibia with cortical destruction (orange arrows). MRI and biopsy were needed to confirm the diagnosis. Figures 22D–F show the corresponding MRI images to this case: **(22D)** Coronal T1-weighted MR image shows the classically low signal of lesion. **(22E)** Sagittal T2-weighted MR image and **(22F)** axial T2-weighted MR image with fat saturation show that the lesion is inhomogeneous.
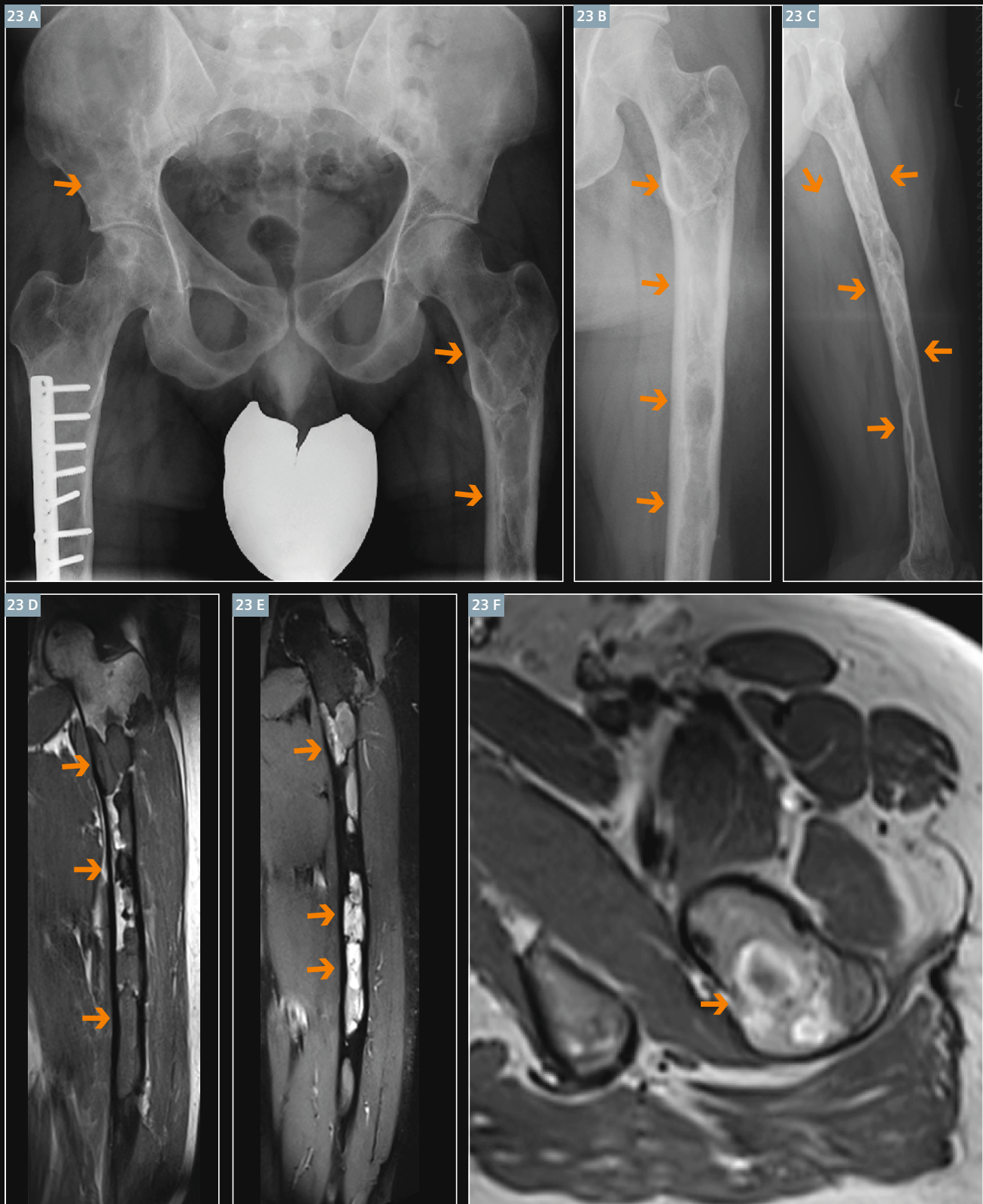
**23** 34-year-old male patient with a polyostotic fibrous dysplasia in pelvis and proximal femur (Albright-syndrome).
**(23A)** Antero-posterior radiograph of the pelvis, **(23B)** antero-posterior radiograph of the left femur and **(23C)** lateral radiograph of the left femur show lots of lesions with smoky appearance in the right os ileum and the left femur (orange arrow).
**(23D)** Coronal T1-weighted MR image of the left femur shows a low signal of the lesions (orange arrow). **(23E)** Coronal STIR MR image of the left femur shows an intermediate to high signal of the lesions (orange arrow) and **(23F)** axial contrast-enhanced T1-weighted MR image shows an inhomogeneous contrast-enhancement of the fibrous tissue (orange arrow).

## Lipoid/fatty type

**Calcaneus lipoma (Fig. 24)**
A common location is the calcaneus. It is a rare entity and a so-called 'leave-me-alone lesion'. Key to diagnosis: Fat signal in all MRI sequences.
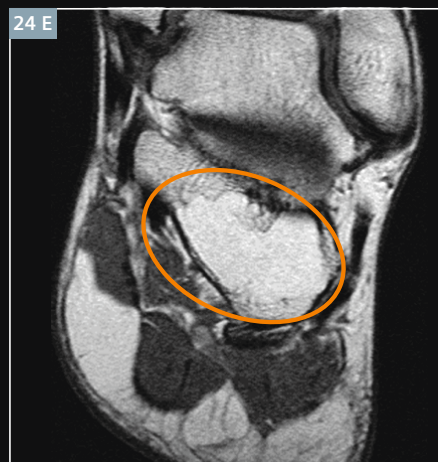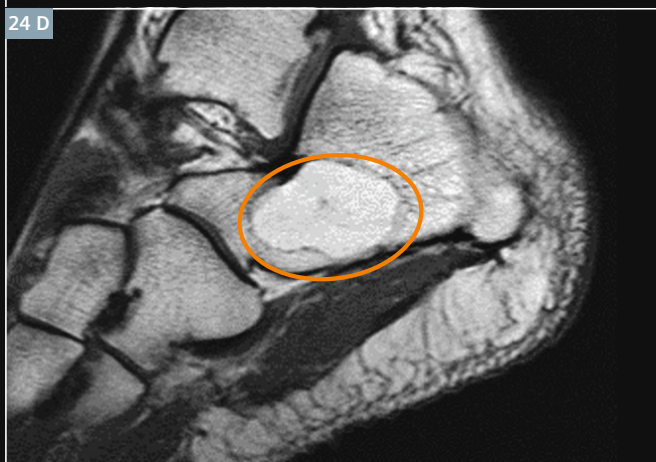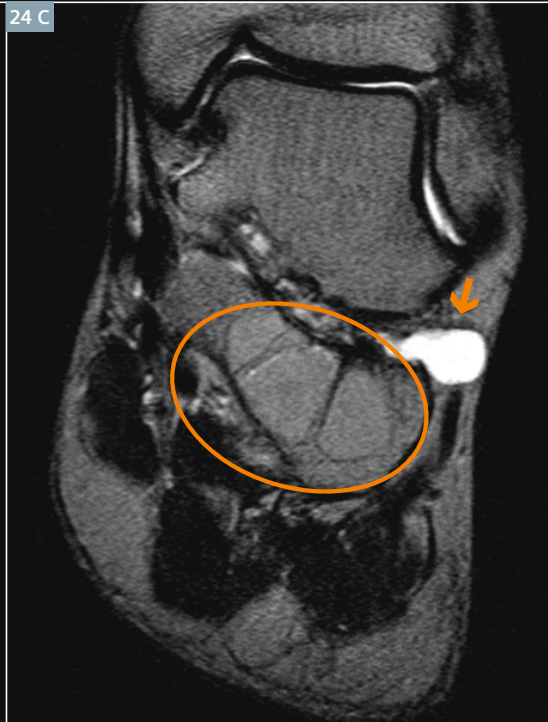


24 49-year-old male patient with an intra-osseous lipoma of the calcaneus as typical location. **(24A)** Lateral radiograph of the calcaneus shows the geographic lesion with sclerotic rim, Lodwick IA (orange arrow). **(24B)** Axial contrast-enhanced T1w MRI with fat saturation, **(24C)** coronal T2w MRI, **(24D)** sagittal T1w MRI and **(24E)** coronal contrast-enhanced T1w MRI. MR images show well that the lesion contains fat, especially seen in 24B and E (orange circle). Notice the synovial cyst between calcaneus and talus in 24C as auxiliary diagnosis (orange arrow).

## Other types

**Solitary bone cyst (Figs. 25, 26)**
Patients are usually younger than
20 years. Common location: calcaneus,
proximal humerus and femur with cen-
tral location of the lesion. Patients have
no pain or periosteal reaction unless
they suffer a fracture through this lesion.
The fracture often produces fragments

that sink to the bottom of the lesion,
well known as the 'fallen fragment
sign' visible on radiographs.

Key to diagnosis: Lytic centrally
located lesion, well-defined with
sclerotic rim (Lodwick type IA). The
MRI shows non-enhancing pure fluid
(in contrary to aneurysmal bone cyst).

If the lesion is located in the calca-
neus think about the differential
diagnosis of an intra-osseous lipoma.
A differentiation by X-ray is then only
possible if the lipoma has a central
calcification. But this differentiation is
not relevant, because both lesions are
'leave-me-alone lesions' [11].
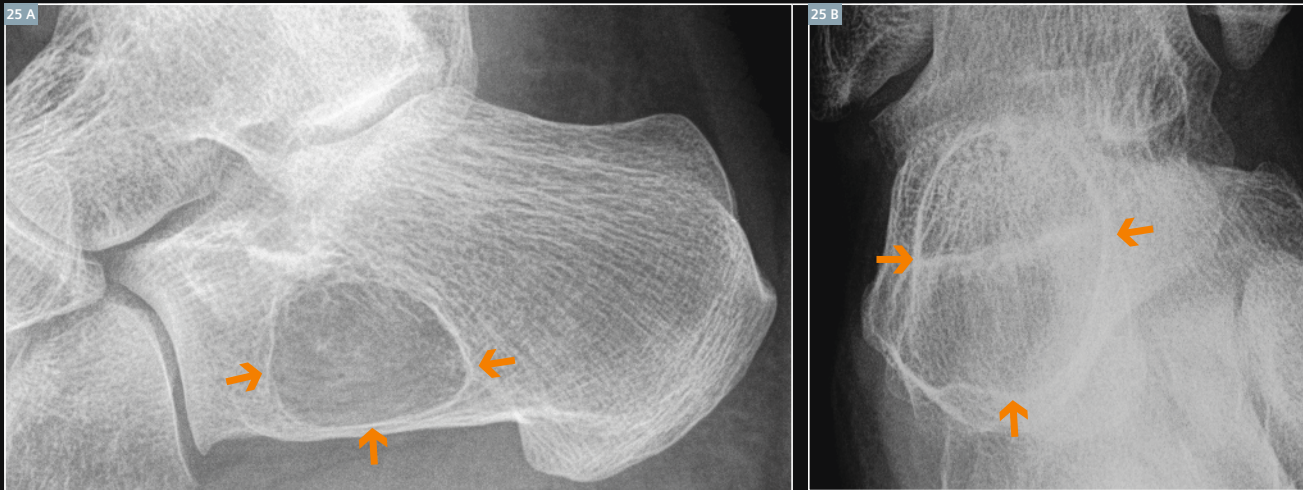


**25** 25-year-old male patient with a solitary bone cyst of the calcaneus. **(25A)** Lateral and **(25B)** antero-posterior radiographs of the calcaneus show both the geographic lesion with sclerotic rim, Lodwick IA (orange arrows). Typically for the location in the anterior to the midportion of the calcaneus and on the inferior border is: only in this position the solitary bone cyst has a characteristic triangular appearance.
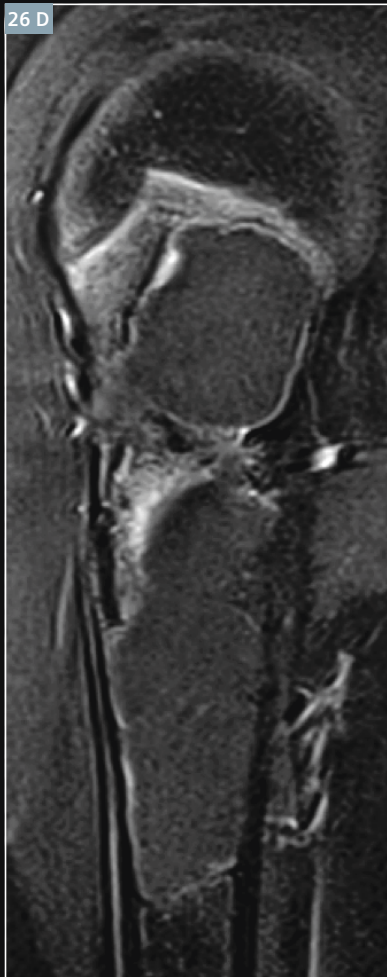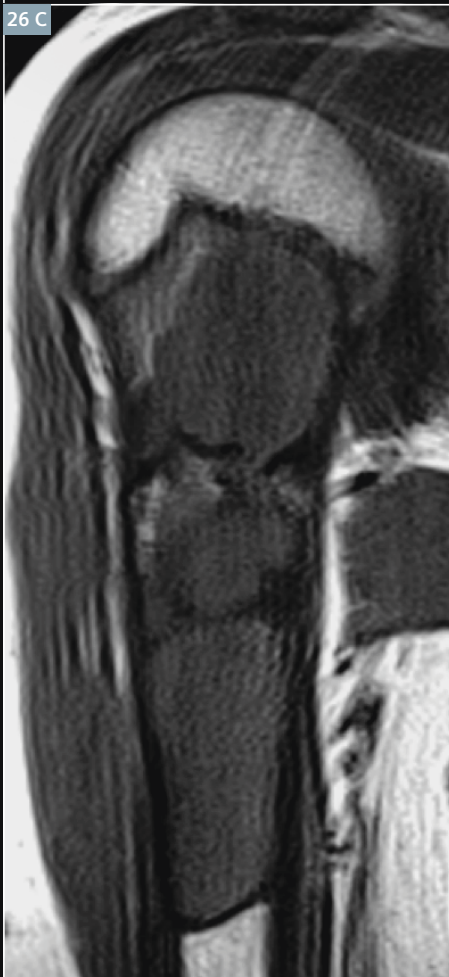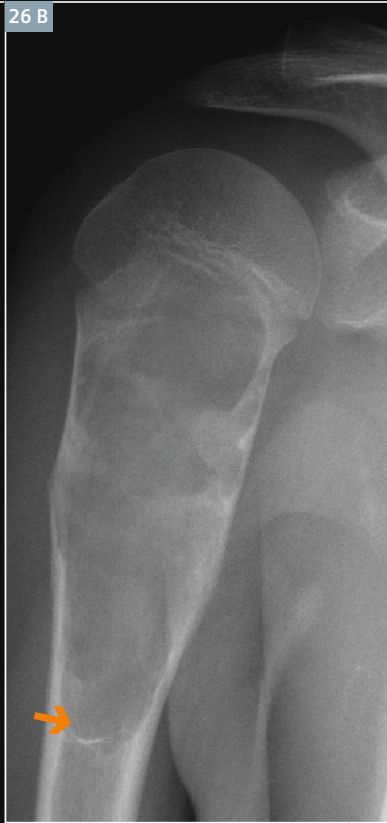
## Save the Date
## 3rd Heidelberg Summer School
## Musculoskeletal Cross Sectional Imaging 2014



July 25/26, 2014
Heidelberg, Germany

Please visit:
www.heidelbergsummerschool.de

26 A



26 B



26

Image gallery of solitary bone cyst with the 'fallen fragment sign'.
**(26A)** Antero-posterior radiograph of the right shoulder of a 9-year-old female patient with the 'fallen fragment sign' in a solitary bone cyst of the humerus (orange arrow).
Figures 26B–E show the case of an 11-year-old patient with a solitary bone cyst also in the right humerus. **(26B)** Antero-posterior radiograph of the right shoulder demonstrates well the pathogno-monic 'fallen fragment sign' of the cystic lesion.

26 C



26 D



**(26C)** Shows a coronal T1w MRI with low signal of the lesion and **(26E)** shows an axial T2w MRI with a small fluid level between the cystic fluid and the blood after the occurred fracture (orange arrow). Usually solitary bone cysts show no fluid-fluid levels as it is typical for the aneurysmal bone cyst.
**(26D)** Coronal contrast-enhanced T1w MRI with fat saturation shows non-enhancing pure fluid.

26 E

## Aneurysmal bone cyst (ABC) (Fig. 27)

The patients are usually younger than 20 years. At the vertebral column, this entity often occurs at the posterior elements of the vertebral bodies.
It shows an aneurysmal, expansive growth with thinned cortex or neo-cortex (ballooned cortices) called 'blow-out' phenomenon in CT.

Key to diagnosis: The aneurysmal bone cyst is a lytic geographic lesion, eccentrically located with extensive thinning of the cortex. Sedimentation effects of blood-filled cysts with fluid-fluid levels and contrast-enhancement of the cystic wall and the septa are typical signs in MRI. If there are solid contrast-enhancing parts consider secondary ABC with other tumors (e.g. giant cell tumor, osteosarcoma, chondrosarcoma, chondroblastoma).
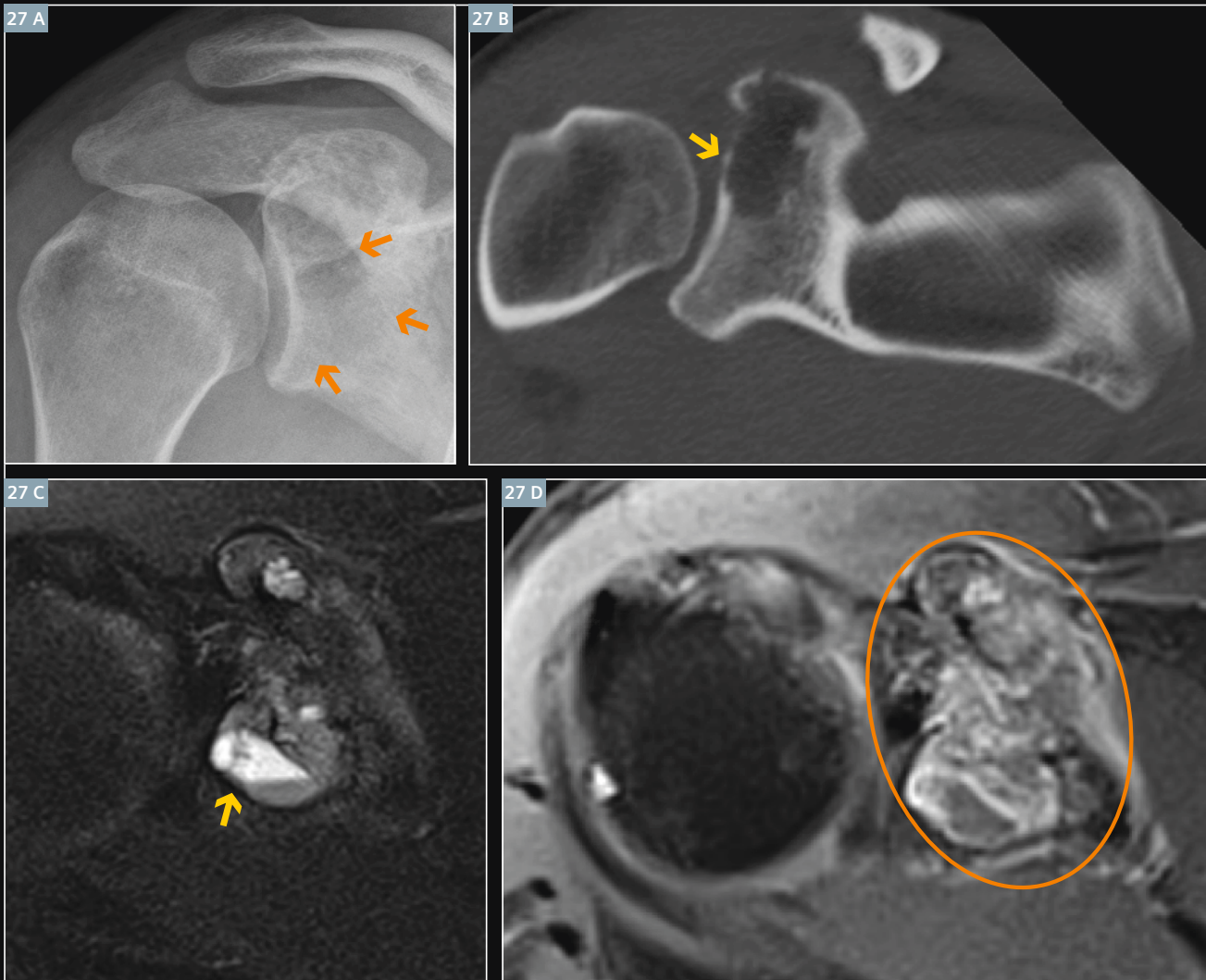


**27** 17-year-old male patient with an aneurysmal bone cyst of the right glenoid. **(27A)** Lateral radiograph of the right shoulder shows a geographic lesion in the glenoid without sclerotic rim, Lodwick IB (orange arrows). **(27B)** Coronal CT of the right shoulder shows a lytic expansible lesion with a thinned cortex (yellow arrow). **(27C)** Axial T2-weighted MRI shows the cystic parts with fluid-fluid level (yellow arrow). **(27D)** Axial contrast-enhanced T1w MRI shows the enhancement of the septa (orange circle).

### Giant cell tumor (Fig. 28)

A precondition is that the epiphysis is closed. This tumour often abuts the articular surface and most often has an eccentric localization. This is often a well defined lesion with a non-sclerotic margin (Lodwick IB). Local aggressive growth and lung metastasis in 5–10% occur.

Key to diagnosis: Osteolytic eccentric, epiphyseal lesion without matrix calcification and extensive thinning of the cortex. The tumor shows low signal in T1-weighting, inhomogeneous or low signal in T2-weighting and contrast-enhancement. If the tumor contains necrosis and hemosiderin, this results in an inhomogeneous contrast-enhancement pattern.
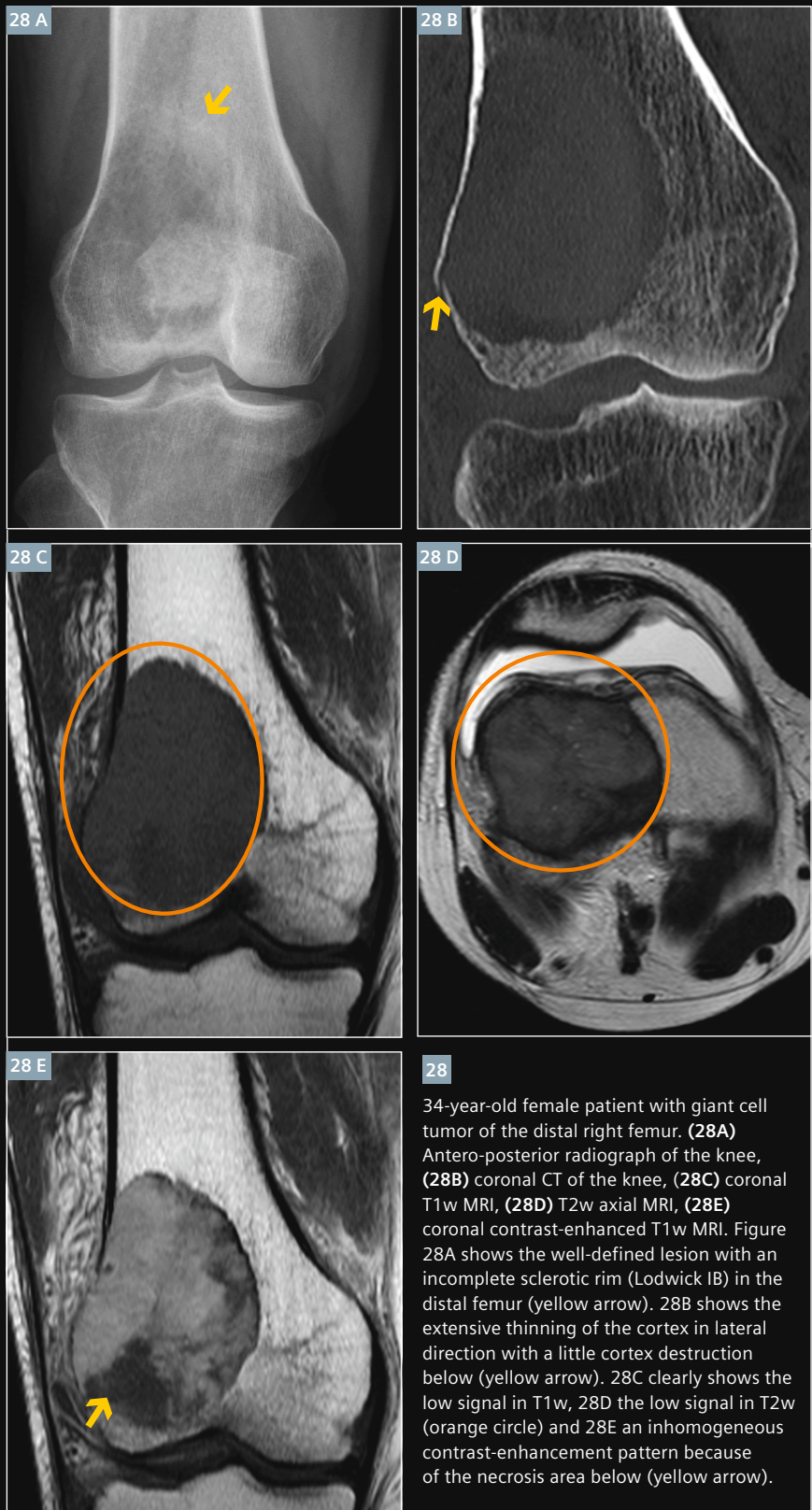
**28**
34-year-old female patient with giant cell tumor of the distal right femur. **(28A)** Antero-posterior radiograph of the knee, **(28B)** coronal CT of the knee, **(28C)** coronal T1w MRI, **(28D)** T2w axial MRI, **(28E)** coronal contrast-enhanced T1w MRI. Figure 28A shows the well-defined lesion with an incomplete sclerotic rim (Lodwick IB) in the distal femur (yellow arrow). 28B shows the extensive thinning of the cortex in lateral direction with a little cortex destruction below (yellow arrow). 28C clearly shows the low signal in T1w, 28D the low signal in T2w (orange circle) and 28E an inhomogeneous contrast-enhancement pattern because of the necrosis area below (yellow arrow).

### Ewing's sarcoma (Figs. 29, 30)

The classic Ewing's sarcoma is a, 'permeative lesion in the diaphysis of long bone in a child', [11], with osteodestruction in CT and a very high signal in T2-weighted imaging indicating infiltration of bone marrow. The location of Ewing's sarcoma tends to follow the distribution of red marrow.

In histology small round blue cells are visible. A large soft tissue mass is possible. Important differential diagnoses are osteomyelitis and eosinophilic granuloma, which have a benign periosteal reaction and sometimes a sequestrum.

Keys to diagnosis are: A permeative lesion or lesion with sclerotic and patchy appearance and periosteal reaction which can be onion-skinned (multilamellated), sunburst or amorphous. Low signal in T1-weighted MR images, high signal in T2-weighted MR imaging with strong contrast-enhancement. More than 50% are osteolytic lesions. Edema and large soft tissue mass often occur.
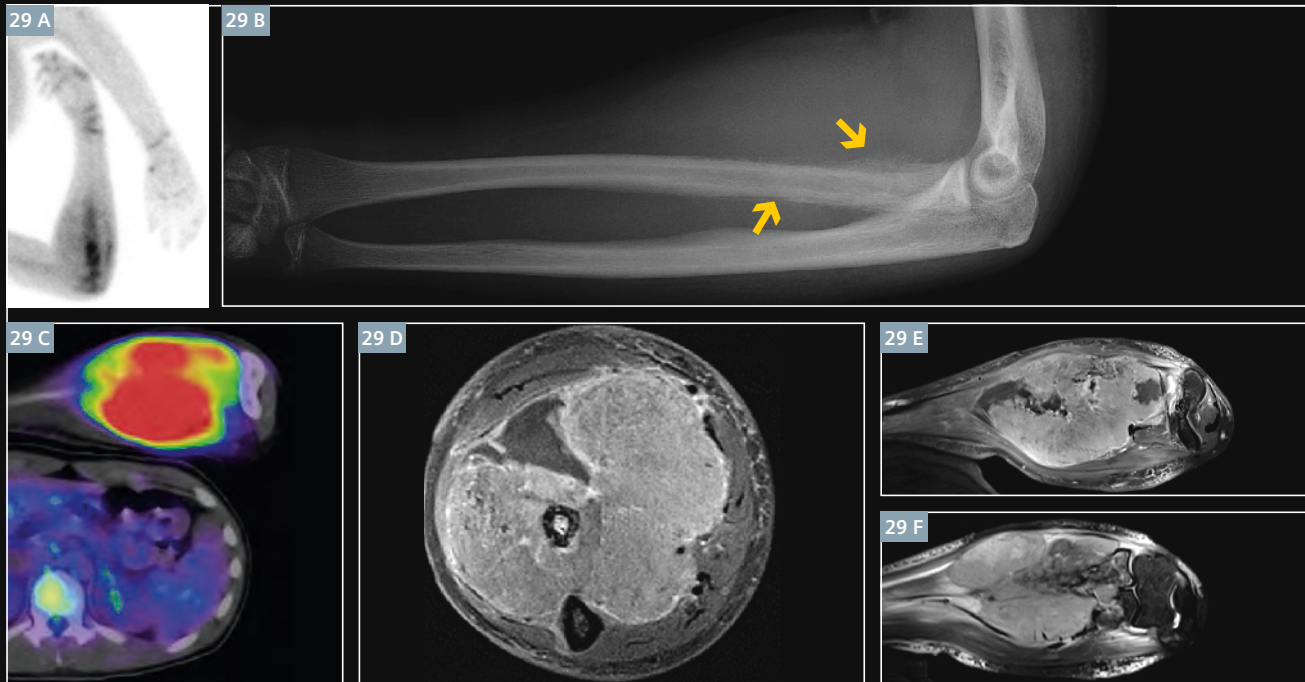


**29** 16-year-old male patient with Ewing's sarcoma of the proximal left forearm. **(29A)** Bone scan shows an overview of the involvement of the proximal radius, the ulna and parts of the distal humerus. **(29B)** Lateral radiograph of the forearm shows the onion-skinned, multilamellated periosteal reaction of the proximal radius (yellow arrows). **(29C)** Three-phase radionuclide bone scan with Tc-99m MDP shows the tracer uptake in the big tumor mass. **(29D, E)** Contrast-enhanced T1-weighted MRI with fat saturation axial (D) and coronal (E) and **(29F)** coronal STIR MRI shows the big tumor involving radius and ulna.
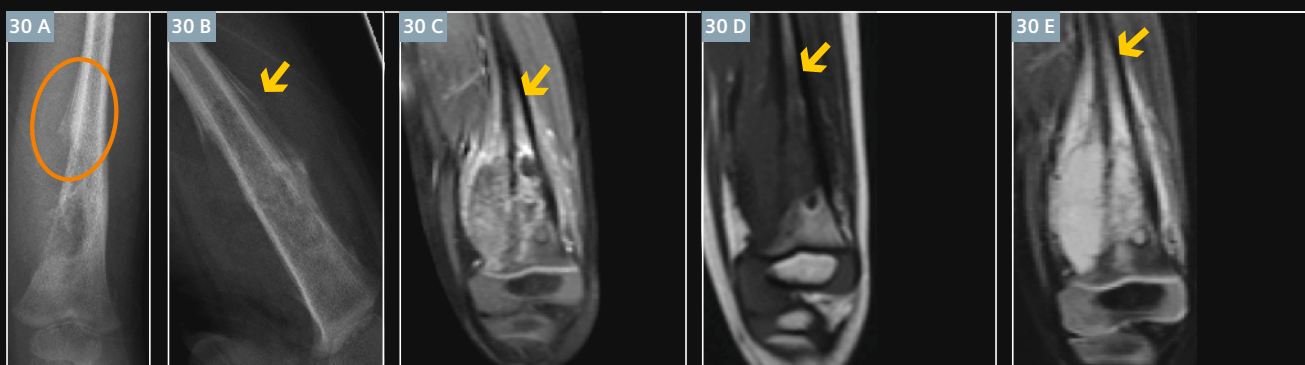


**30** 3-year-old male patient with Ewing's sarcoma of the left distal femur. **(30A)** Antero-posterior radiograph of the femur, **(30B)** lateral radiograph of the femur, **(30C)** coronal contrast-enhanced T1-weighted MRI with fat saturation, **(30D)** coronal T1-weighted MRI, **(30E)** coronal STIR MRI. Figure 30A clearly shows the Codman-triangle, whereby the elevated periosteum forms an angle with the cortex, (orange circle) and 30B the onion-skinned periosteal reaction (yellow arrow). Figures 30C–E show the T1w hypo-, T2w hyperintense signal character of the tumor with contrast-enhancement, the large soft tissue component (yellow arrows) and also the Codman triangle.
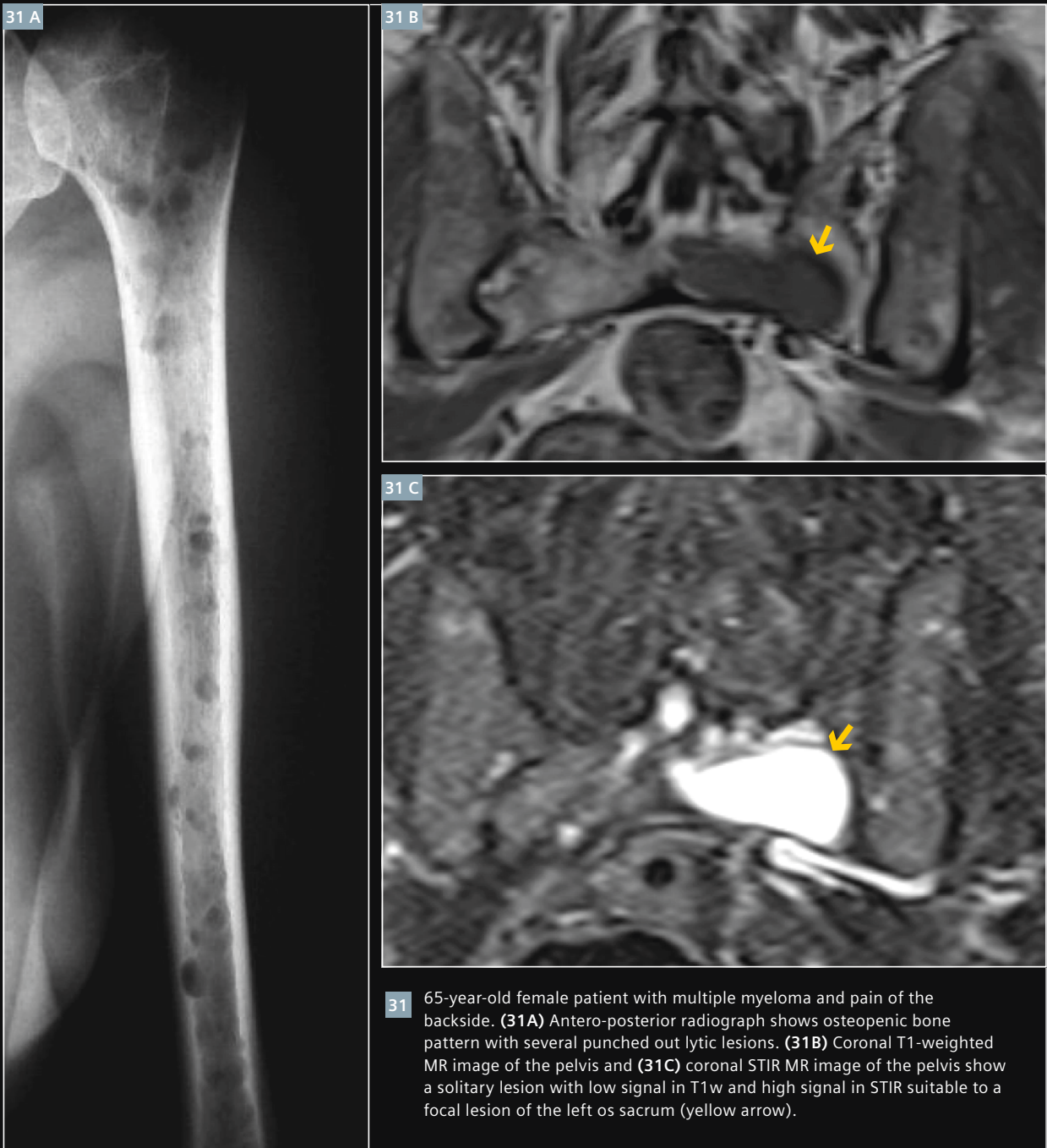
## Multiple myeloma (Fig. 31)

In multiple myeloma, a proliferation of monoclonal plasma cells within the bone marrow occurs. The vertebral column is mostly affected and 70% of patients are older than 60 years. Multiple lytic lesions in an adult older than 40 years almost always suggest metastases or multiple myeloma. Bone sarcomas are rare, and the most common cause of a solitary destructive lesion in an adult is a metastasis. Low-dose CT is important for proving osteolytic lesions and MRI [22] for proving bone marrow affection: Decrease of T1-weighted signal in bone marrow infiltration compared to the disks, and a signal increase in the STIR images compared to muscle tissue. Whole-body MRI is suitable for demonstration of the tumor burden. It is important to think of patient's age when interpreting T1-weighted MR imaging, because young patients still have a cell-rich red bone marrow and therefore also a low T1 signal. We differentiate three patterns of bone marrow infiltration: diffuse, multifocal, or 'salt-and-pepper' pattern. Salt-and-pepper pattern indicates a low grade disease stadium. A single lesion is called plasmacytoma [22, 23].

**31** 65-year-old female patient with multiple myeloma and pain of the backside. **(31A)** Antero-posterior radiograph shows osteopenic bone pattern with several punched out lytic lesions. **(31B)** Coronal T1-weighted MR image of the pelvis and **(31C)** coronal STIR MR image of the pelvis show a solitary lesion with low signal in T1w and high signal in STIR suitable to a focal lesion of the left os sacrum (yellow arrow).

## Metastases (Fig. 32)

40% of all metastases are located in the vertebral column. The most frequent primary tumors are lung, breast, prostate, renal cell, gastrointestinal and thyroid carcinomas. Bone marrow infiltration happens before osseous destruction. It is important to pay attention to fractures, spinal canal invasion and myelon compression.

Key to diagnosis: For the diagnosis of bone metastases a low signal in T1-weighted MR images is more sensitive than osteolysis in CT [24]. Osteolytic metastases have a high signal in T2-weighted images, whereas osteoblastic metastases have a low to isointense signal in T2-weighted images. Take into account these factors in older patients and consider several osteoblastic and/or osteolytic lesions.

32 C

Head R lat    Head L lat

Thorax R V L    Thorax L D R

Pelvis R V L    Pelvis L D R
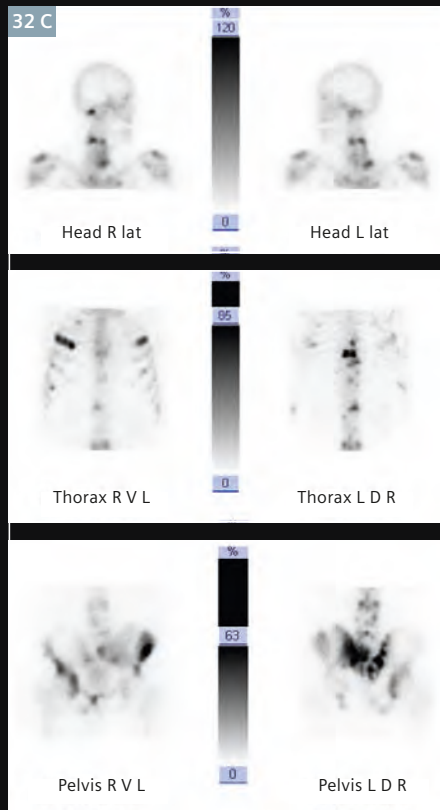
**32**

55-year-old man with osteoblastic metastases of vertebral column and pelvis in prostate cancer. **(32A)** Lateral radiograph of the vertebral column, **(32B)** antero-posterior radiograph of the lower vertebral column and os sacrum show several osteoblastic metastases of the vertebral bodies and the os sacrum. **(32C)** Scintigraphic bone scan shows more skeletal metastases.

32 A

32 B
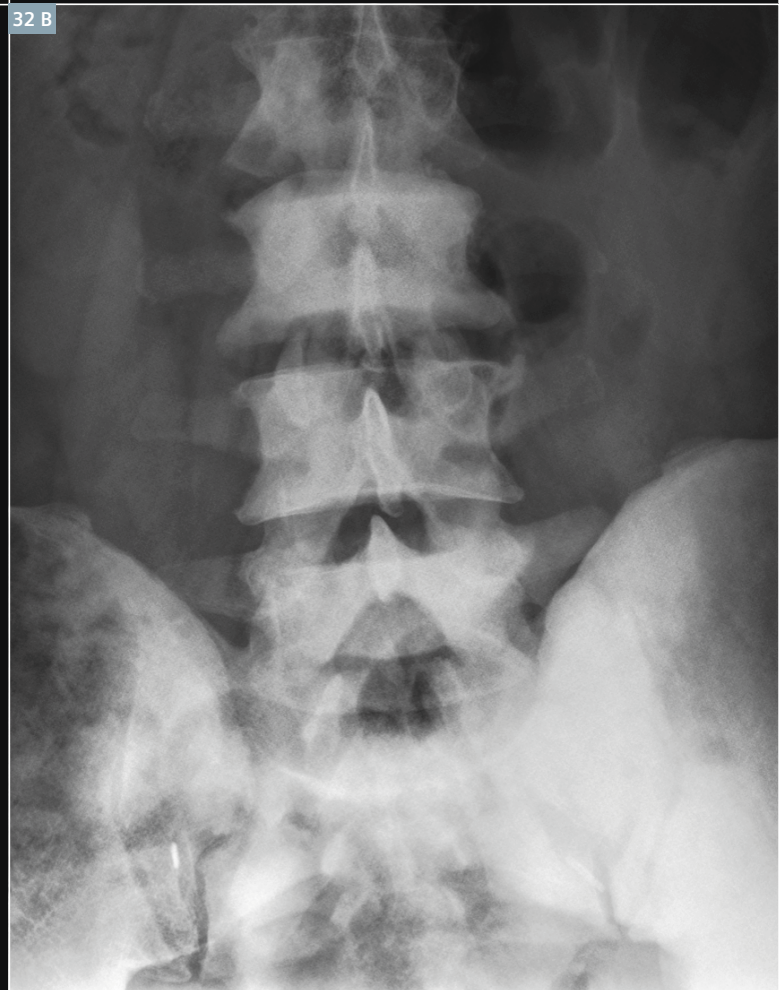
## Summary

### Role of X-ray

In addition to patient history and clinical findings, a radiograph in two orthogonal planes is still of great importance for determining the Lodwick classification and the tumor matrix, whereas the bone matrix is only poorly visualized in X-ray: You cannot differentiate between lesions containing fluid and solid lesions without mineralized matrix. In general, conventional X-ray radiography is the starting point and CT and MR images should only be interpreted with concurrent radiographic correlation.

### Role of CT

CT is superior to MRI for the assessment of mineralized structures especially cortical integrity, matrix mineralization, and periosteal reactions [21]. Small lucency of the cortex, localized involvement of the soft tissues, and thin peripheral periosteal reaction can be best seen with CT [16]. CT is the examination of choice in the diagnosis of the nidus of osteoid osteoma in dense bone [17]. CT is valuable in the diagnosis of tumors of the axial skeleton such as spinal metastasis as well as in systemic staging.

### Role of MRI [18-21]

Without any radiation MRI can be helpful while evaluating lesions that represent a differential diagnosis dilemma between benign and malignant lesions before a biopsy. For example in aneurysmal bone cysts MRI can display fluid levels in blood filled cavities better than CT. Another example, MRI before biopsy for staging all suspected sarcomas of bone could help identifying extraosseous sarcoma better. MRI plays an important role in planning limb salvage surgeries because of its superior role for soft tissue evaluation including the presence or absence of neurovascular invasion [21]. MRI helps by identifying skip lesions and helps measure the thickness of cartilage cap. The cap is thin in benign lesions and thicker in chondrosarcomas [14, 15]. This aids evaluation of the entire compartment of long bones in acceptable time. (Important here is a large field-of- view of the MR sequence, see Fig. 33.) This in turn helps to improve the quality of life by reducing morbidity without affecting survival. MRI is most useful in evaluation of spine metastasis differentiating osteoporotic and metastatic compression fractures. In Multiple Myeloma cases whole-body MRI scans are suitable for demonstration of the tumor burden. Though not yet in clinical routine, newer techniques such as diffusion-weighted imaging and DCE-MRI may support assessment of tumor response. More studies are being conducted.
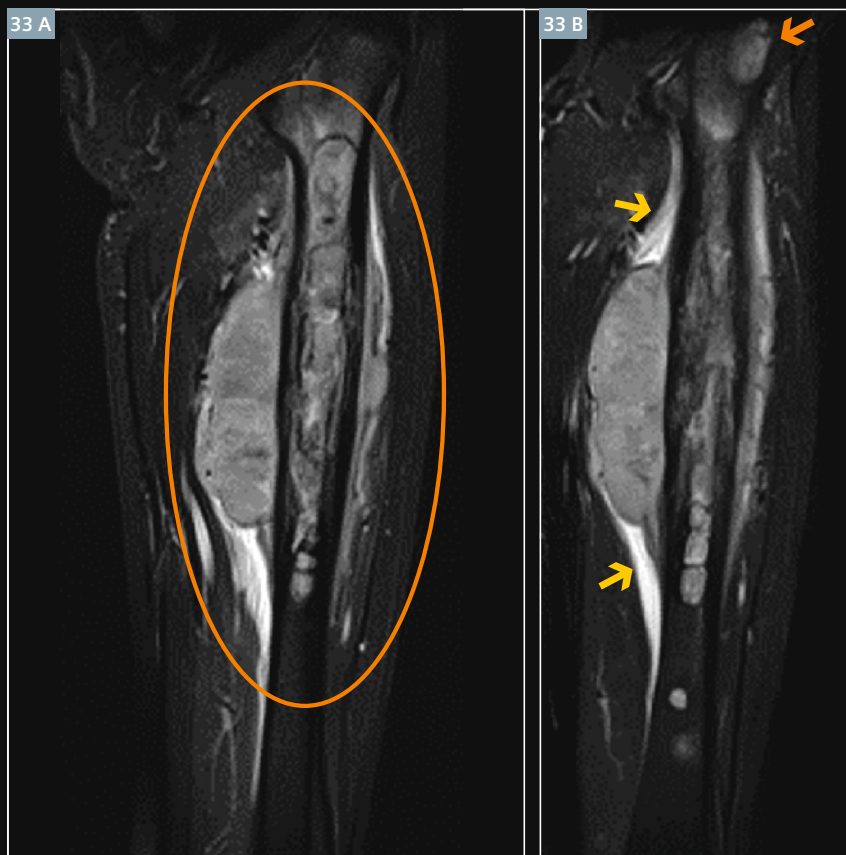
**33** 13-year-old female patient with Ewing's sarcoma. **(33A, B)** Coronal STIR MR images show the tumor in the left femur diaphysis (orange circle) with a large soft tissue mass surrounded by a soft tissue edema (yellow arrows) and a skip lesion in the femoral neck (orange arrow).

## Proposed tumor MRI protocol

### Sequences unenhanced

- coronal STIR with a large field-of-view
- coronal T1-weighted TSE (turbo spin echo)
- axial T2-weighted TSE with fat saturation
- sagittal T2-weighted TSE

### Contrast-agent (0.1 mmol/kg body weight)

- axial contrast-enhanced T1-weighted TSE with fat saturation
- coronal contrast-enhanced T1-weigthed TSE + subtraction (contrast-enhanced minus native T1-weighted MRI scan)

The contrast-enhanced sequences are important in biopsy planning for identifying necrotic and viable tumor tissue. The biopsy should be targeted to the viable tumor area.

### Optional

- MR-angiography
- Dynamic T1-weighted contrast-enhanced MRI (DCE-MRI)

Dynamic sequences are important for biopsy planning to identify vital tumor tissue [19-21], to which the biopsy should be guided.

**References**

1 WHO classification of bone tumours 2006.

2 Vanel D, Ruggieri P, Ferrari S, Picci P, Gambarotti M, Staals E, Alberghini M. The incidental skeletal lesion: ignore or explore? Cancer Imaging. 2009 Oct 2; 9 Spec No A: S38-43.

3 Lodwick GS, Wilson AJ, Farrell C, Virtama P, Dittrich F. Determining growth rates of focal lesions of bone from radiographs. Radiology 1980; 134: 577-583.

4 Erlemann R. Basic diagnostics of bone tumors. Radiologe 2009; 49: 257–267.

5 Oudenhoven LF, Dhondt E, Kahn S, Nieborg A, Kroon HM, Hogendoorn PC, Gielen JL, Bloem JL, De Schepper A. Accuracy of radiography in grading and tissue-specific diagnosis-a study of 200 consecutive bone tumors of the hand. Skeletal Radiol. 2006; 35: 78-87.

6 Miller T. Bone tumors and tumorlike conditions: analysis with conventional radiography. Radiology 2008; 246: 662-674.

7 Lucas DR, Unni KK, McLeod RA, O'Connor MI, Sim FH. Osteoblastoma: clinicopathologic study of 306 cases. Hum Pathol. 1994 Feb;25(2):117-34.

8 Rehnitz C, Sprengel SD, Lehner B, Ludwig K, Omlor G, Merle C, Kauczor HU, Ewerbeck V, Weber MA. CT-guided radiofrequency ablation of osteoid osteoma and osteoblastoma: clinical success and long-term follow up in 77 patients. Eur J Radiol 2012 Nov;81(11):3426-34. doi: 10.1016/j. ejrad.2012.04.037. Epub 2012 Jul 6.

9 Rehnitz C, Sprengel SD, Lehner B, Ludwig K, Omlor G, Merle C, Kauczor HU, Ewerbeck V, Weber MA. CT-guided radiofrequency ablation of osteoid osteoma: correlation of clinical outcome and imaging features. Diagn Interv Radiol. 2013 Jul-Aug;19(4):330-9. doi: 10.5152/dir.2013.096.

10 Omlor GW, Lehner B, Wiedenhöfer B, Deininger C, Weber MA, Rehnitz C. [Radiofrequency ablation in spinal osteoid osteoma. Options and limits]. [Article in German]. Orthopade. 2012 Aug;41(8):618-22. doi: 10.1007/s00132-012-1907-x.

11 Clyde A. Helms, Fundamentals of Skeletal Radiology (2005),3. Edition, Elsevier inc.

12 Murphey MD, Robbin MR, McRae GA, Flemming DJ, Temple HT, Kransdorf MJ. The many faces of osteosarcoma. Radiographics 1997; 17: 1205-1231.

13 Kloth JK, Wolf M, Rehnitz C, Lehner B, Wiedenhöfer B, Weber MA. [Radiological diagnostics of spinal tumors. Part 1: general tumor diagnostics and special diagnostics of extradural tumors]. Orthopade. 2012 Aug;41(8):595-607. doi: 10.1007/s00132-012-1978-8. [Article in German].

14 Murphey MD, Choi JJ, Kransdorf MJ, Flemming DJ, Gannon FH. Imaging of osteochondroma: variants and complications with radiologic-pathologic correlation. Radiographics. 2000 Sep-Oct;20(5):1407-34.

15 Bernard SA, Murphey MD, Flemming DJ, Kransdorf MJ. Improved differentiation of benign osteochondromas from secondary condrosarcomas with standardized measurement of cartilage cap at CT and MR imaging. Radiology 2010 Jun;255(3):857-65.

16 Brown KT, Kattapuram SV, Rosenthal DI. Computed tomography analysis of bone tumors: patterns of cortical destruction and soft tissue extension. Skeletal Radiol 1986; 15: 448-451).

17 Glass RB, Poznanski AK, Fisher MR, Shkolnik A, Dias L. MR imaging of osteoid osteoma. J Comput Assist Tomogr 1986; 10: 1065-1067.

18 Anderson SE, Steinbach LS, Schlicht S, Powell G, Davies M, Choong P. Magnetic resonance imaging of bone tumors and joints. Top Magn Reson Imaging. 2007 Dec; 18(6):457-65.

19 Fayad LM, Jacobs MA, Wang X, Carrini JA, Bluemke DA. Musculoskeletal tumours: how to use anatomic, functional, and metabolic MR techniques. Radiology 2012; 265: 340-356.

20 Alyas F, James SL, Davies AM, Saifuddin A. The role of MR imaging in the diagnostic characterisation of appendicular bone tumours and tumour-like conditions. Eur Radiol 2007; 17: 2675-2686.

21 Roberts CC, Liu PT, Wenger DE. Musculoskeletal tumor imaging, biopsy, and therapies: self-assessment module. AJR Am J Roentgenol. 2009; 193(6 Suppl): S74-78.

22 Fechtner K, Hillengass J, Delorme S, Heiss C, Neben K, Goldschmidt H, Kauczor HU, Weber MA. Staging monoclonal plasma cell disease: comparison of the Durie-Salmon and the Durie-Salmon PLUS staging systems. Radiology. 2010 Oct; 257(1):195-204. doi: 10.1148/radiol.10091809.

23 Bäuerle T, Hillengass J, Fechtner K, Zechmann CM, Grenacher L, Moehler TM, Christiane H, Wagner-Gund B, Neben K, Kauczor HU, Goldschmidt H, Delorme S. Multiple myeloma and monoclonal gammopathy of undetermined significance: importance of whole-body versus spinal MR imaging. Radiology. 2009 Aug; 252(2):477-85. doi: 10.1148/radiol.2522081756.

24 Bohndorf K, et al. Radiologische Diagnostik der Knochen und Gelenke. (2006) 2nd edition, Thieme.

## Contact

Katharina Grünberg, M.D.
Section Musculoskeletal Radiology
Diagnostic and Interventional Radiology
University Hospital Heidelberg
Schlierbacher Landstraße 200a
69118 Heidelberg
Germany
Katharina.Gruenberg@med.uni-heidelberg.de